

Article

Modular Level Power Electronics (MLPE) Based Distributed PV System for Partial Shaded Conditions

Sajid Sarwar ¹, Muhammad Yaqoob Javed ^{1,*}, Mujtaba Hussain Jaffery ¹, Muhammad Saqib Ashraf ²,
Muhammad Talha Naveed ¹ and Muhammad Annas Hafeez ¹

¹ Department of Electrical and Computer Engineering, COMSATS University Islamabad, Lahore 54000, Pakistan; engsajidsarwar@gmail.com (S.S.); m.jaffery@cuilahore.edu.pk (M.H.J.); talha586p@gmail.com (M.T.N.); m.annas13@yahoo.com (M.A.H.)

² Department of Electrical Engineering, Government College University, Faisalabad 38000, Pakistan; saqibdogar@outlook.com

* Correspondence: yaqoob.javed@cuilahore.edu.pk

Abstract: Photovoltaic (PV) solar energy is a very promising renewable energy technology, as solar PV systems are less efficient because of climate conditions, temperature, and irradiance change. So, to resolve this problem, two PV topologies are used, i.e., centralized and distributed PV systems. The centralized technique is quicker than the distributed technique in terms of convergence speed and a faster power tracking approach. In the event of uniform irradiance, the centralized system also has the benefit of supplying superior energy, but in PS scenarios, a huge amount of energy is lost. However, the distributed approach requires current and voltage measurements at each panel, resulting in a massive data set. Nevertheless, in the event of shading circumstances, the distributed technique is highly effective because a modular level power electronics (MLPE) converter is used. While in a centralized PV system, there is only a single DC-DC converter for the whole PV system. In this research work, a DFO-based DC-DC converter is designed for modular level, with an ability to perform a rapid shutdown of the module under fire hazard conditions, troubleshooting, and monitoring of a module in a very efficient way. The robustness of the proposed MPPT DFO algorithm is tested with different techniques such as Cuckoo Search (CS), Fruit Fly Optimization (FFO), Particle swarm optimization (PSO), Incremental conductance (InC), and Perturb and observe (P&O) techniques. The proposed technique shows better results in terms of MPPT efficiency, dynamic responsiveness, and harmonics. Furthermore, the result of MLPE and the centralized system is verified by using the Helioscope with different inverter companies like SMA, Tigo, Enphase, Solar edge, and Huawei. The results prove that MLPE is a better option in the case of shading region for attaining the maximum power point.

Keywords: MLPE; photovoltaic; MPPT; dragonfly algorithm; partial shading condition; uniform irradiance condition



Citation: Sarwar, S.; Javed, M.Y.; Jaffery, M.H.; Ashraf, M.S.; Naveed, M.T.; Hafeez, M.A. Modular Level Power Electronics (MLPE) Based Distributed PV System for Partial Shaded Conditions. *Energies* **2022**, *15*, 4797. <https://doi.org/10.3390/en15134797>

Academic Editors: Pedro Dinis Gaspar, Pedro Dinho da Silva and Luís C. Pires

Received: 2 May 2022
Accepted: 20 June 2022
Published: 30 June 2022

Publisher's Note: MDPI stays neutral with regard to jurisdictional claims in published maps and institutional affiliations.



Copyright: © 2022 by the authors. Licensee MDPI, Basel, Switzerland. This article is an open access article distributed under the terms and conditions of the Creative Commons Attribution (CC BY) license (<https://creativecommons.org/licenses/by/4.0/>).

1. Introduction

In the past decades, scarcity of fossil energy and focus on environmental damage have become two major challenges affecting people's lifestyles. As a result, most countries are currently researching and expanding renewable energy sources (RES). The energy produced from RES like wind, geothermal heat, sunlight, and heat are the natural source of energy. Unlike diminishing conventional fossil fuels, RES is replenished naturally and will be considered limitless. RES harvest energy without the harmful effects of pollution. A major part of RES comes from biomass and wind. In the coming years due to the recent advancements in the technology of solar, PV energy has resulted in admirable growth of the PV Solar business, which is expected to outperform other RES. PV power production has several advantages over other RES, especially in terms of durability, operation, and integration. Among these, the best alternative is solar power [1,2].

Several grid-connected solar installations use a centralized control scheme. Furthermore, the mismatches, deterioration, or partially shaded impact of a panel is a very remarkably power loss issue faced by a PV system [3]. As a result, the power pattern of a PV system has several maximum power points (MPP), indicating that distributed system is very efficient [4,5].

MPPT techniques have been developed for the last two decades to force the PV devices to operate at maximum power point. The researcher employs several MPPT approaches in the PV system. For detecting the Global Maximum Power Point (GMPP), P-V and I-V characteristics will be used [6,7].

These techniques' characteristics are judged based on speed, accuracy, and complexity. Some MPPT techniques are discussed in the literature such as traditional techniques are fractional open-circuit voltage (FOCV) [8] and fractional short circuit current (FSCC) [9]. The most commonly used is perturb and observe (P&O) technique [10]. However, this scheme is not able to find MPPT in partial shading conditions, but the computation technique incremental conductance (InC) method is accurate but can be expensive [11]. The conventional DMPP algorithms for the photovoltaic system give the maximum output for UI conditions. However, for PS conditions, the output is found in the vicinity of local maxima. Moreover, soft computing techniques are used for both PS and UI conditions. However, these techniques are complex, and they require a lot of time to track GM. Therefore, it cannot be implemented in a low-cost controller. So, a novel, fast, efficient, and appropriate DMPP control algorithm for both the centralized and decentralized as well as the distributed photovoltaic system is required to be developed [12,13].

The desired algorithm may feature less computational burden and complexity compared to the already available techniques in the literature. Furthermore, the DMPP techniques should give the advantages of both soft computing and conventional DMPP algorithms [14]. The optimization methods for MPPT in PV systems include Artificial Bee Colony (ABC) [15], Ant Colony Optimization (ACO) [16], Genetic Algorithm (GA) [17], Differential Evolution (DE) [18], Grey Wolf Optimization (GFO) [19], and Cuckoo's Search (CS) [20]. The PV system's efficiencies have been rated based on reaction speed, accuracy, efficiency, partial shading, and performance under quick response. Until recently, no technique has consistently produced the greatest outcomes. Table 1 shows the comparisons of several MPPT approaches. SAPVS and GCPVS are the abbreviations for Standalone PV System and Grid-connected PV System, respectively, in Table 1.

There is no set criteria for determining which method is the best. Each technique has advantages and disadvantages. It is attempted to rate or score each strategy regarding the performance metrics listed in Table 1. It will assist the reader in judging and selecting an approach that is preferable to others. The following are the scoring criteria:

- From 1 to 3 score on a scale, all evaluation parameters are rated.
- Score is given to 3 in case of sensors needed = 1, otherwise the score granted is 1, if the number of sensors needed to is more than 1.
- Scores for tracking speed, accuracy and level of complexity are given as the following criteria: high = 1, medium = 2 and low = 3.
- If any technique is efficient for partial shading, then the score is given to 3, otherwise the score is granted to 1.
- Total score allotted = tracking speed (score) + efficient for partial shading (score) + settling time (score) + (accuracy) + sensed variables (score).

Table 1. Performance comparison of MPPT techniques.

Sr No.	Ref. No.	Year	MPPT Method	Tracking Accuracy	Efficient for Partial Shading	Converter Type	Variable Sensed	Type of PV System Used	Can Be Implement in Low-Cost Controller	Tracking Speed	Level of Complexity	Total Score = 15
1	[8]	2016	FOCV	Medium/2	No/1	Boost	V/3	SAPVS	Yes	Medium/2	Low/3	11
2	[9]	2021	FSCC	Medium/2	No/1	Boost	I/3	SAPVS	Yes	Medium/2	Low/3	11
3	[10]	2019	P&O	Medium/2	No/1	Boost	I,V/1	GCPVS	Yes	Fast/3	Low/3	10
4	[11]	2019	InC	High/3	Yes/3	Boost	I,V/1	SAPVS	Yes	Fast/3	Medium/2	12
5	[21]	2020	PSO	Medium/2	Yes/3	Buck-Boost	I,V/1	GCPVS	No	Medium/2	Low/3	11
6	[22]	2018	FP	High/3	Yes/3	Buck	I,V/1	SAPVS	No	Fast/3	Low/3	13
7	[23]	2019	ANN	High3	Yes/3	Buck	I,V/1	SAPVS	Yes	Medium/2	Low/3	12
8	[24]	2022	SMC	High/3	Yes/3	Boost	I,V/1	SAPVS	No	Fast/3	Medium/2	12
9	[15]	2022	ABC	High/3	Yes/3	Boost	I,V/1	GCPVS	No	Medium/2	Low/3	12
10	[16]	2021	ACO	High/3	Yes/3	Boost	I,V/1	SAPVS	No	Fast/3	Low/3	13
11	[20]	2020	CS	High/3	Yes/3	SEPIC	I,V/1	SAPVS	No	Fast/3	High/1	11
12	[17]	2022	GA	Medium/2	Yes/3	Buck-Boost	I,V/1	GCPVS	Yes	Medium/2	Low/3	11
13	[18]	2018	DE	High/3	Yes/3	Boost	I,V/1	GCPVS	No	Medium/2	Low/3	12
14	[19]	2019	GWO	High/3	Yes/3	Buck	I,V/1	SAPVS	No	Fast/3	Medium/2	12
15	[25]	2017	GSO	Medium/2	Yes/3	Boost	I,V/1	GCPVS	Yes	Fast/3	Low/3	12
16	[26]	2018	TCA	High/3	Yes/3	Boost	I,V/1	SAPVS	No	Fast/3	Medium/2	12
17	[27]	2020	SSO	High/3	Yes/3	Boost	I,V/1	SAPVS	No	Fast/3	Low/3	13
18	[28]	2022	OTCA	High/3	Yes/3	Boost	I,V/1	SAPVS	No	Fast/3	Low/3	13
19	[29]	2017	JayaDe	Low/1	Yes/3	Boost	I,V/1	SAPVS	No	Medium/2	Low/3	10
20	[30]	2018	SA	High/3	Yes/3	Boost	I,V/1	GCPVS	No	Low/1	Medium/2	10
21	[31]	2020	FFO	High/3	Yes/3	Boost	I,V/1	GCPVS	No	Medium/2	Low/3	12
22	[32]	2017	CSO	High/3	Yes/3	Boost	I,V/1	SAPVS	No	Medium/2	Medium/2	11
23	[33]	2019	HHO	High/3	Yes/3	Boost	I,V/1	SAPVS	No	Fast/3	Low/3	13

There are three types of PV systems that are commonly used in the PV market, i.e., string inverter, micro-inverter, and inverter with power optimizer. A string inverter is the most used technology because it is efficient and cost-effective. In string inverter, a string of several PV-modules is connected to one inverter with a single-phase grid connection [34,35]. There are some technical issues with it. In each string, all the PV panels have similar orientation and tilt angles. Secondly, if there is PS in the PV module, then that PV module is bypassed, and the output of the string is reduced. So, to resolve these issues, Modular Level Power Electronic (MLPE) devices are introduced [36,37].

The commonly used MLPE devices are the Modular Level Inverter (MicroInverter) and Modular Level Converter (Power Optimizer). MLPE devices resolve both issues of a string inverter, but these systems are costly [38]. Another additive advantage is that an MLPE device can provide modular level rapid shutdown (Safety Feature), design flexibility, and Modular Level energy monitoring, remote management, and troubleshooting.

As a result, to increase the power from the PV system in the event of shade, an MLPE device could be used to acquire the maximum output from the panel. Micro-inverters and power optimizers can be used with MLPE to increase the efficiency of the solar PV system in specific scenarios. By removing the unmatching, the optimizer boosts the PV system's generating capacity [39].

The main contribution of our work is that MLPE performs and gives better efficiency to the Solar distributed PV system.

- A mathematical model is designed to identify the uniform irradiance (UI), and partial shading (PS) conditions in centralized and MLPE distributed PV systems across different MPPT techniques.
- We compare the proposed DFO approach with five other methods, including InC, FFO, CS, PSO, and P&O, in order to determine its robustness and power efficiency.
- MLPE will assist in meeting newer National Electrical Code (NEC) regulations for the quick shutdown of power PV circuits.

The effects of centralized and distributed PV systems on power under partially shaded situations are explored in this research. It shows a comparison as well as a thorough study of the combination of centralized and distributed PV systems. Furthermore, the maximum PV serving ability may be estimated safely in a cluster-based PV system.

The remainder of the paper is laid out as follows: Section 1 gives an introduction and literature review. A detailed description of the MLPE distributed PV system is illustrated in Section 2. Practical verification of MPPT through hardware is given in Section 3. Section 4 discuss proposed MPPT techniques and calculation for the shading technique. Simulink model designing and implementation are presented in Section 5. Section 6 elaborated on results and discussion. Section 7 presents the efficiency and analysis of the PV system. Comparative analysis of MLPE distributed and centralized PV systems are expressed in Section 8. Section 9 described the Helioscope results. Concluding remarks are illustrated in Section 10. Future work is given in Section 11.

Boost Converter

In PV power systems, the DC-DC converter is an essential component of the output power. A buck, boost, or buck–boost converter are some of the most popular converters used in a PV system to change the power output value. According to the system's needs, they reduce or increase the power rating. The boost converter outperforms all other DC to DC converters in terms of voltage management, power, and efficiency in achieving the desired results. The output voltages of a PV energy system should be adjusted by altering the switching frequency of a DC-DC boost converter [35,40–44]. The output voltage and connected load must be coordinated to achieve this.

Capacitance output, duty-cycle, capacitance input, and inductance of the converter mathematical equations are given below:

$$Cap_{out} = \frac{I_*}{f_{swi}8\Delta V_{rip,load}} \quad (1)$$

$$Cap_{in} = \frac{\Delta I_{rip}}{f_{swi}8\Delta V_{rip,pv}} \quad (2)$$

$$V_{output} = \frac{V_{input}}{-dc + 1} \quad (3)$$

$$L_{induc} = \frac{dcI_o}{\Delta I_{Load}2f_{swi}} \quad (4)$$

$$dc = \frac{T_{on}}{T_{swi}} \quad (5)$$

where V_{input} is the input voltage, f_{swi} represents the switching frequency, I_{rip} denotes the ripple current and dc elaborates the duty cycle of a DC-DC boost converter. Traditional PV technologies may be trapped on LM and fail to achieve GM for the total highest energy collection. As a result, bio-inspired strategies are being applied in this study to find the MPP.

2. Detailed Description of MLPE Distributed PV System

PV modules are often connected in series or parallel formation to make a string, which is then hooked up to form an array, in order to obtain high layered DC voltage. Because the entire array of PV is controlled at one site for grid connection, these installations are classified as centralized PV systems [4,12,45,46]. PV systems require high electrical performance overall, but are seen to be useless for renewable power collecting in a variety of non-ideal situations [47]. In the situation of mismatched operating circumstances, PV systems consisting of strings of PV panels parallel connected and powering a central DC/AC inverter are inefficient in terms of energy produced. The centralized-based PV system that is illustrated in Figure 1.

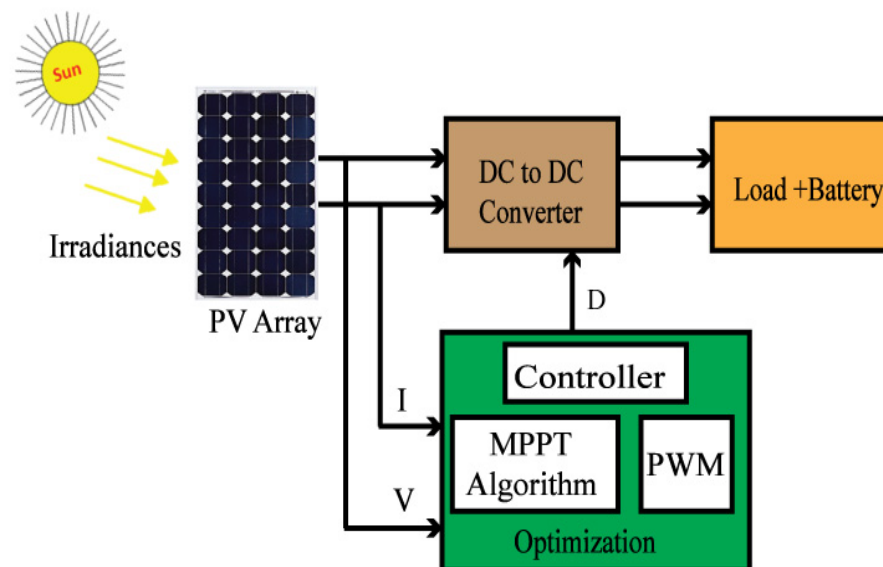


Figure 1. Centralized PV system.

The tracing of the MPP of the power and the voltage (P-V) profile of the entire PV field may collapse due to the existence of by-pass diodes, which causes such a P-V characteristic to have multiple peaks. In this instance, MPPT techniques are unable to track to exact MPP [48–52].

DMPPT systems have been presented at various levels of detail to solve the imbalance problem. String-level, submodule-level, module-level, and cell-level precision are all

included in the architecture of DMPPT PV designs. DMPPT [53] helps you to get around the problems that come with mismatching. One alternative DMPPT approach is to use a DC to DC converter for each PV module to execute MPPT. DC to DC converter output channels are linked in series, and the resulting strings drive a centralized inverter as elaborated in Figure 2.

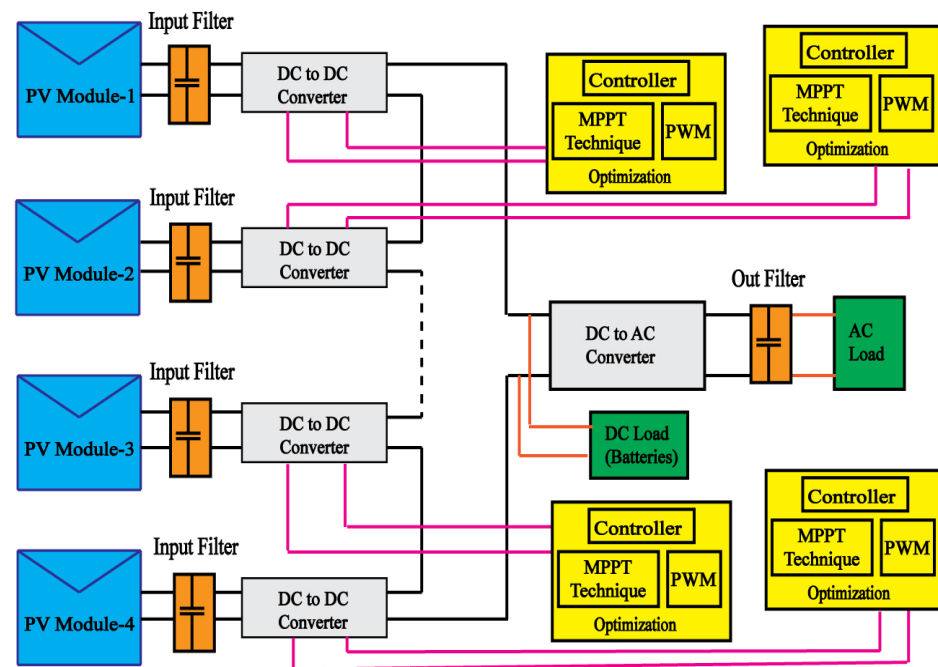


Figure 2. MLPE Distributed PV system.

The following are some examples of electronic applications created using such an architecture, etc., Solar Edge Power Box, Enphase, Huawei, and Tigo Energy Module Maximizers. The PV system can be divided into two types:

1. Standalone: The output power inverter is linked with the local demands in these devices.
2. Grid-tied system: The output power inverter in such setups is combined with the AC Electrical public grid.

There are several possible circuit topologies for PV systems.

1. Centralized PV: In this output is connected and DC power is delivered to one converter.
2. String topology: When several PV panels are connected in rows and each row has its inverter.
3. Modular topology: In this topology, each PV module is connected to one inverter.

In DMPPT, PV panels have connected in series with a power optimizer and micro-inverter on each panel. A power prediction model is required to estimate the baseline maximum load. PV power to be observed by direct control of power control scheme which is a DC-DC converter. For this purpose, MLPE can be used to create a DC power optimization. The optimizer can work in either move step-up or down mode.

2.1. Shading in PV System

Solar panels in the uniform solar irradiance condition have the same irradiance values. It monitors the several irradiance levels in the partially shaded condition. Because of the PS, a succession of PV modules connected together may have low current and low performance. A string is made up of many PV modules combined and connected in series to boost voltages. A single inverter is used to connect multiple strings.

However, because of varying irradiance conditions, a non-uniform condition may cause non-matching and hot-spot problems. By attaching a by-pass diode, which provides an additional channel for the flow of greater current from other PV panels, these impacts

can be minimized. PV array of 4×1 of same and different irradiance levels is shown in Figure 3A,B, respectively. PS is affected by the MPPT issue, which leads to a PV power system with a low-performance efficiency. Traditional techniques such as InC and P&O handle this issue because their judgments are based on favorable and unfavorable gradients [54]. These methods may not be able to distinguish between alone GM and an LM that only works in one location. PS, on the other hand, produces multiple peaks on the curve, putting the efficiency of these traditional algorithms at risk. For PV power systems, bio-inspired techniques can efficiently find GM [55–57].

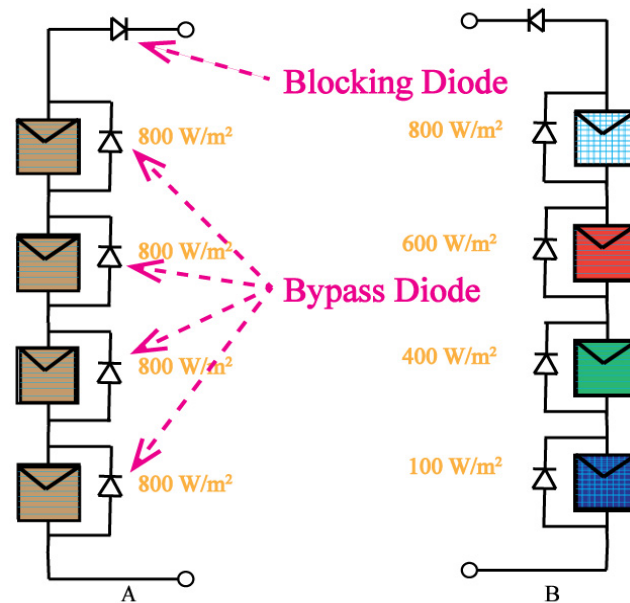


Figure 3. (A) Uniform irradiance case. (B) Partial shading case.

Power losses are a big issue under varying irradiance circumstances, and they can be mitigated with MPPT approaches because PS affects the system process performance greatly. To address this issue, MPPT approaches are being used. Traditional gradient-based MPPT approaches like P&O and InC can't tell the difference between GM and LM. These strategies can only work on a single point, and the selection is solely based on whether the gradient is favorable or unfavorable. The effectiveness of such gradient-based approaches is severely harmed since PS generates several peak locations on the slopes. Bio-inspired optimization strategies have been effectively used for PV MPPT applications and have the potential to find the GM.

2.2. Calculation of Shading Losses

To determine the number of shade losses that can be retrieved using MLPE in a specific use situation, multiply the number of shade losses by the variety of uses. A Shade Mitigation Factor (*SMF*) is calculated using the significant variation in total energy. The proportion of shading losses can be recovered by using MLPE in a specific use situation. *SMF* is defined as follows:

$$SMF = \frac{-Energy_{REF} + Energy_{MLPE}}{-Energy_{REF} + Energy_{unshade}} \quad (6)$$

The amount of the *SMF* value for a specific MLPE has the advantage of not being highly dependent on the degree of the shade being analyzed (light vs. heavy). Well over three-shade graphs utilized in the investigation, an average value can be determined. This *SMF* value can be directly compared to the yearly review performance of a traditional inverter system with one with the MLPE. The modeling software like PV-watts is used to find the performance efficiency [58].

$$\text{Actual Shading Derate} = [(-SMF + 1)(\text{shading loss})] \quad (7)$$

Because there is ambiguity in the computation of the *SMF* and the Shading Losses percentage, so a rough approximation can be made. Instead of a percentage for electrical loss in performance, shade losses are usually expressed as a percentage of solar irradiance loss [59].

3. Practical Verification of MPPT through Hardware

A hardware setup is implemented to check the response of commercial inverters for both uniform and partial shading conditions. Figure 4 depicted the complete experimental implementation setup. The Magna power PV simulator (TSD100-15/380+HS) is used for PV panel simulation, Infini hybrid inverter 10 kW is used for DC/AC conversion, and the 5 kW lithium-ion batteries and 5 kW R_L load are also used. Two different scenarios are implemented to check the MPP tracking of the PV inverter.

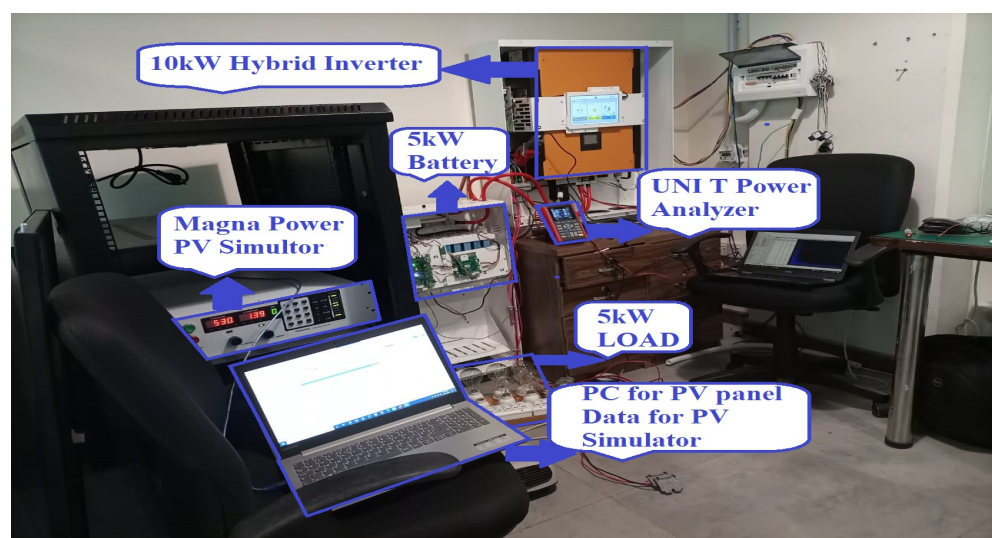


Figure 4. Complete hardware implementation setup.

The tracking of MPPT for Uniform irradiance and partial shading conditions is shown in Figures 5 and 6, respectively. The MPPT algorithm in the inverter perfectly detects global maxima in UIC but in PS conditions, it is stuck in any local maxima. So, it indicates that the algorithm used in the inverter is a conventional algorithm and it is not designed for partial shading problems. The power loss due to partial shading is up to 70% [60].

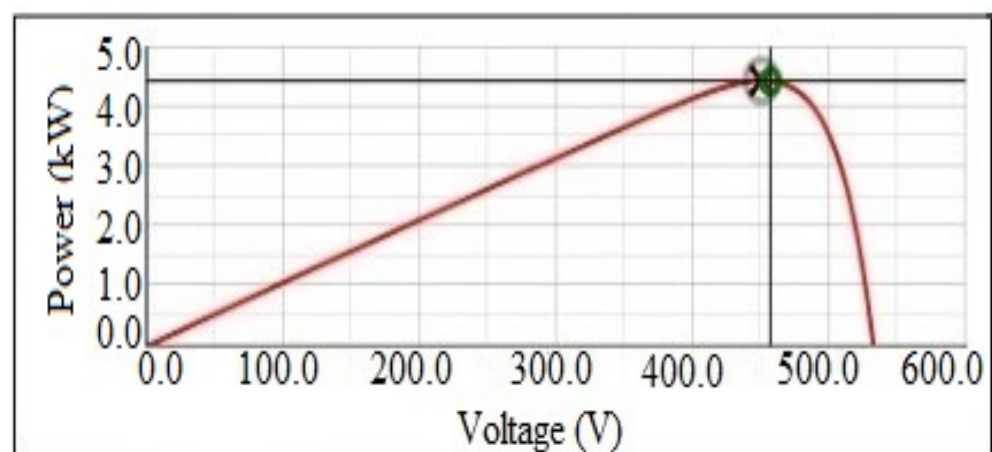


Figure 5. P-V curve for UI condition.

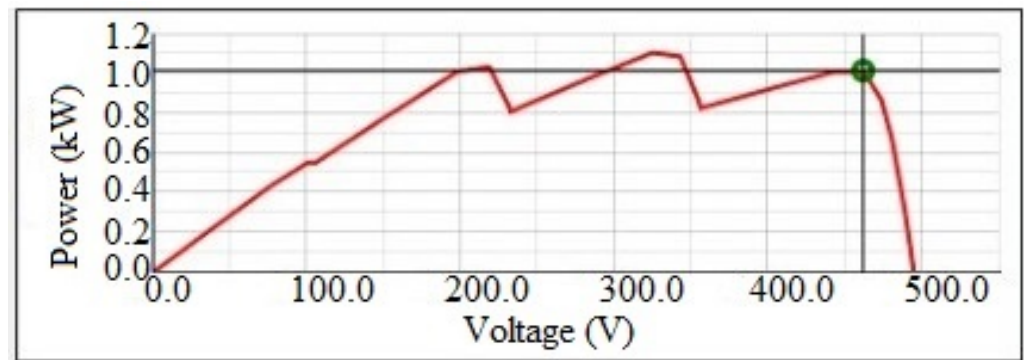


Figure 6. P-V curve for PS condition.

4. Proposed MPPT Techniques

The DF algorithm helps to track the most optimal peak height considerably more efficiently. The other bio-inspired strategies and other standard techniques have been presented as an MPPT method suitable for DMPPT purposes. The primitive process of the DFO technique is illustrated in Figure 7.

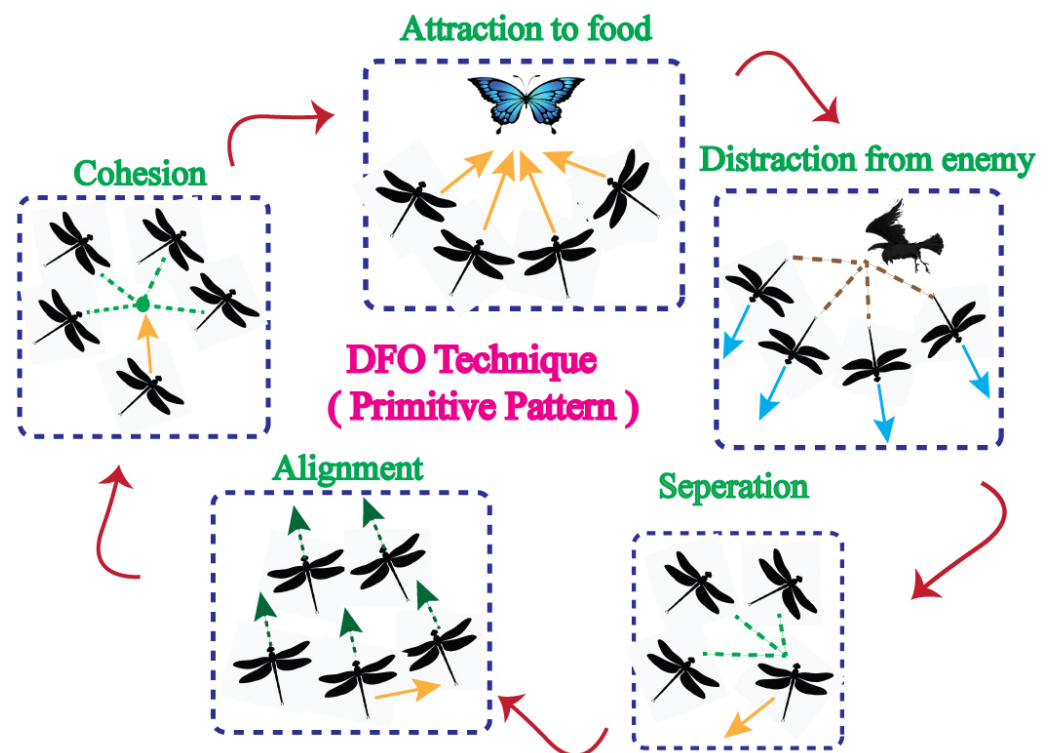


Figure 7. DFO technique primitive process.

DF's Algorithm can be expressed using the mathematical form. The motion in the swarm can be decided by behavior such as separation, alignment, cohesion, food, and enemy [61].

1. First step is the separation of the dragon fly, which means that any DF does not collapse with the other fly. In case of a static swam, it denotes the current position of the dragonfly where the position is denoted by k th. Separation S_k for individuals k th can be calculated with $S_k = -\sum_{(N=1)}^X (Q - Q_N)$, where Q and Q_N indicate the N th nearby DF, and X shows the total number of different neighbors.

2. The alignment that indicates how well the DF's velocity corresponds to the velocity of persons in the same region, where Alignments is denoted by A_j , and it can be calculated as $\sum_{(N=1)}^X * V_k$. Where V_k is the velocity of the k th neighboring DF.
3. The cohesion, which means the ability of the DF to move about the mid-point of the mass of neighbors. Cohesion can be represented by C_k and it can be written as the equation $C_k = \frac{\sum_{(N=1)}^X Q_N}{X} - Q$, where Q denotes the real position of individual DFs and Q_N represents the N th position of the neighboring DF.
4. The individuals of DF move towards food, which is most important for the sake of survival. The attraction of food for the DFs can be found as F_k at position y is shown $F_k = Q_{food} + Q$. The placement of food location is denoted by Q_{food} , and Q refers to the present position of the individual.
5. Every person moves far from the rival, as indicated by the enemy's label, and their formula can be written as $E_k = Q_{enemy} + Q$. Where Q_{enemy} denotes the enemy's location and Q denotes the participant's location. These five sources finalize the current individual's position. The final upgraded position can be calculated as $Q_k = Q_i + \Delta Q_k$. The values of ΔQ can be found out as

$$\Delta Q_k = (sS_k + aA_k + cC_k + fF_k + eE_k) + W\Delta Q_k \quad (8)$$

where, s denoted the weight of separation, S_k represent the separation of i th DF, a denoted the weight of alignment step, A_k stands for i th alignment of DF algorithm, c denotes the cohesion's weight, C_k elaborates the k th DF's cohesiveness, f represents the food weighing factor, k_k indicates the k th food of DFs, e denotes the enemy weighting element, and E_k serves the k th opponent of DF. The flowchart of the DFO technique is given in Figure 8.

P-V curve tracer can also be drawn for making the extracting energy much more visible in the case of the centralized and distributed system. In the case of a centralized PV system, the different peaks in the local and global maxima appear on the tracer. The local maxima show the MPPT point, which results in the case of decaying values and the global maxima show the one peak carrying the higher values. The pseudocode of the DF is shown in Algorithm 1 [61]. The algorithm feature is to track the global maxima from the peaks. However, the distributed PV system has an advantage over a centralized system as it makes a single peak for a single panel and can extract power from every single panel even if it is low.

Algorithm 1 Pseudocode of DF algorithm [61].

Create the k_i population of DF's ($k = 1, 2, \dots, n$).

Initiate Q_k ($k = 1, 2, \dots, n$) step vectors.

while The final condition is unsatisfactory.

Determine all of the DF's performance indices.

Upgrade the enemies and food sources.

Values of (w), (s), (a), (c), (f), and (e) could be brought up to date.

Determine values of (S), (A), (C), (F), and (E) employing their formulas.

Change the neighborhood's radius.

if A DF is neighboring by a minimum one other DF.

Upgraded the velocity.

Based on $Q_k = Q_k + \Delta Q_k$, position of vector are now upgraded.

else

Position of vectors are upgraded.

end if

Look and adjust the new locations depending on the variable limits.

end while

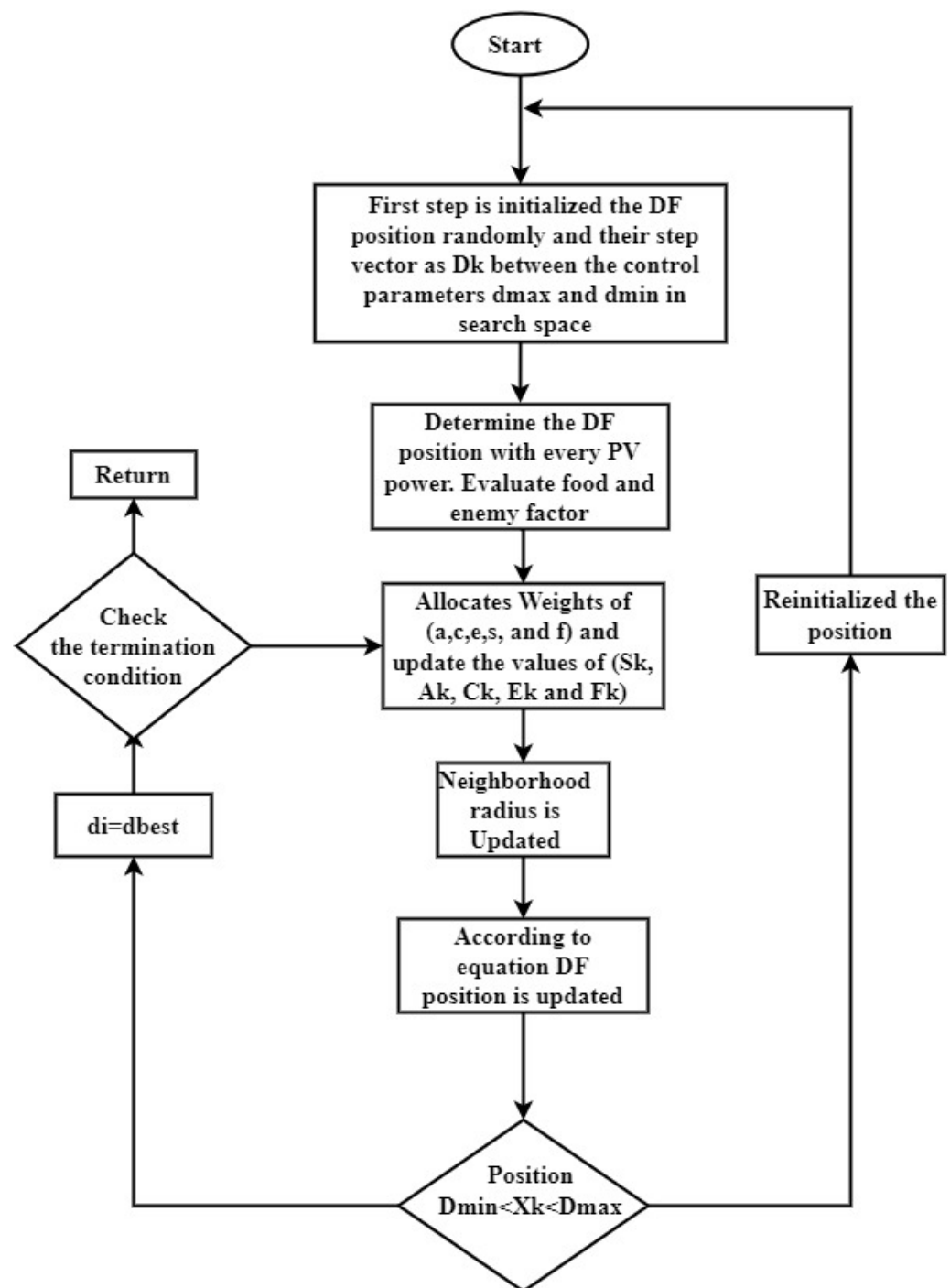


Figure 8. Flowchart of DFO technique.

For the last two decades, MPPT approaches have been designed to force PV systems to run at their MPP [62]. The investigator employs a variety of MPPT approaches in the PV system. P-V and I-V characteristics will be employed to detect the GMPP. The qualities of these approaches are judged based on their efficiency, accuracy, and complexity [63]. Old methods, such as fractional open-circuit voltage (FOCV) [64] and fractional short circuit current (FSCC) [11], are classical techniques. The most widely used approach is P&O [65]. However, this methodology fails to detect MPPT in partial shade situations [43]. The conventional DMPP algorithms for the PV system give the maximum output for UI conditions. However, for PS conditions, the output is found in the vicinity of local minima. Moreover, soft computing techniques are used for both PS conditions and UI conditions. But these techniques are complex, and it requires a lot of time to track GM.

Therefore, it cannot be implemented in a low-cost controller. So, a novel, fast, efficient, and appropriate DMPP control algorithm for both the centralized and decentralized as well as the distributed photovoltaic system is required to be developed.

5. Simulink Model Designing and Implementation

For comparing the performance of the centralized and distributive system, design the Simulink model through Matlab software. PV curve tracers of Centralized and MLPE distributed PV systems are also made for the purpose of searching for the maximum value from the PV array.

5.1. Simulink Model of Curve Tracer and Centralized PV System

In a Centralized PV system, a single converter and single inverter are used for implementation. The first step of implementation for a centralized PV system is to design the PV curve tracer, which means finding the maximum value from the PV array. After that, find the maximum point of local and global maxima in order to design the centralized model. The MPPT algorithm is used to find the GM from the PV array and extract the output. The PV curve tracer implemented in the model in Simulink is shown Figure 9.

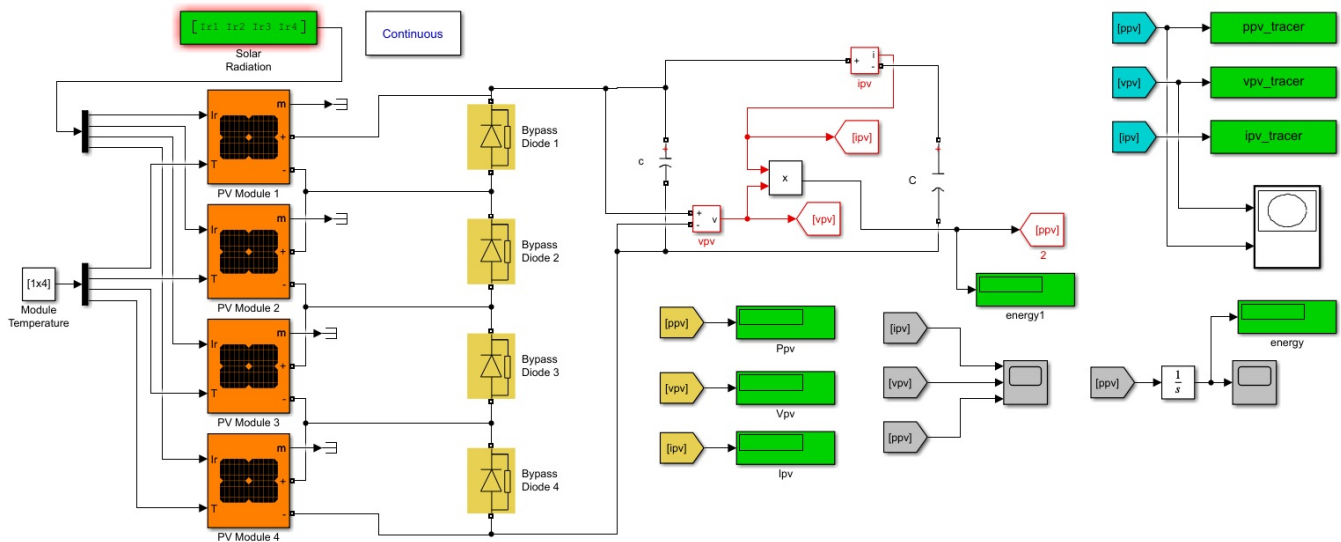


Figure 9. Simulink model of curve tracer for centralized PV system.

The PV array, which is connected with the bypass diode that allows the module to bypass in case of shading, and all four panels are connected in series taking temperature and irradiance as input and computing the output. After designing the Simulink model for PV curve trace and finding the maximum PV value, design their controller and converter. The Simulink model of the centralized PV system is shown in Figure 10.

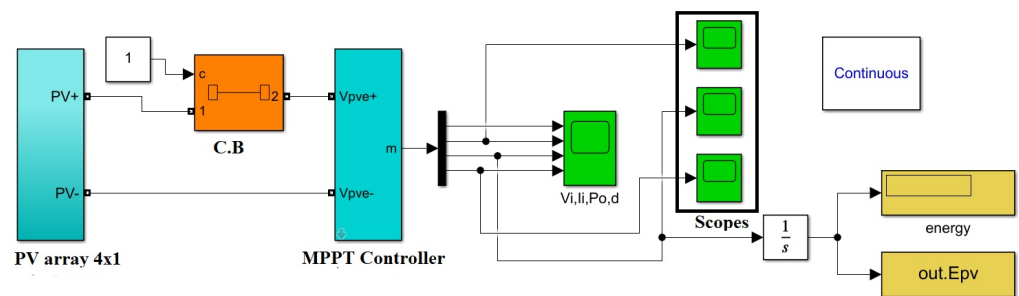


Figure 10. Complete Simulink model of centralized PV system.

In the Simulink model of the centralized PV system, different cases of irradiance with respect to their irradiance level are made. PV array is connected to a single DC-DC converter. The result can be divided into four different cases. The pattern of UI and PS are described that are taken in Table 2. Case 1 describes the partial shading such as 800, 600, 400 and 100. Case 2 describes the partial shading 800, 600, 400, and 400. Case 3 describes the shading on two panels as 800, 800, 600, and 600. Case 4 describes the uniform irradiance on all panels.

Table 2. P-V and I-V characteristic curves at different irradiance values centralized PV system.

Case	Irradiance S_i (W/m ²)				$Power_{max}$
Case 1 PS1	PV-1:800	PV-2:600	PV-3:400	PV-4:100	375 W
Case 2 PS2	PV-1:800	PV-2:600	PV-3:400	PV-4:400	494 W
Case 3 PS3	PV-1:800	PV-2:800	PV-3:600	PV-4:600	740 W
Case 4 UI	PV-1:800	PV-2:800	PV-3:800	PV-4:800	940 W

5.2. Simulink Model of Curve Tracer and MLPE Distributed PV System

In the case of the distributed PV system, it has multiple converters. Each string is connected in series and every converter has its own MPPT, which helps to utilize the power from each panel in case of shading regions. For this purpose, the design of the PV Curve tracer of the MLPE distributed PV system is shown in Figure 11 as the design in the centralized PV system. The different peak occurs on different panels concerning their irradiance level and utilized 25 to 35% more power during irradiance condition as compared to centralized and decentralized system tracers.

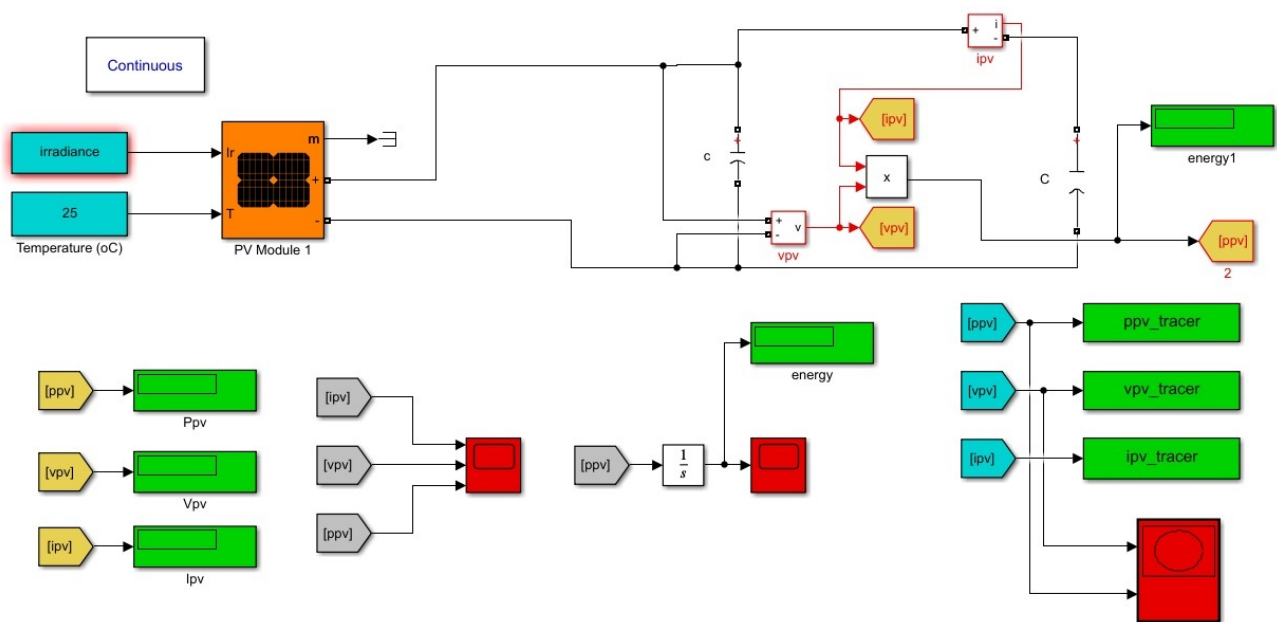


Figure 11. Simulink model of curve tracer for MLPE distributed PV system.

Make different cases of shading for the MLPE distributed PV system in order to compare it with the centralized PV system. The different irradiance patterns of UI and PS cases are elaborated in Table 3.

In the PV curve tracer of the MLPE distributed PV system, find the peaks on different irradiance levels. Such a system is designed on 800, 600, 400, and 100 irradiance bases. Cases can be made on these irradiances, and UI is considered as 800 while low irradiance is 100. The distributed PV system can be tested on different MPPT algorithms on four panels array-like CS, FFO, PSO, DF, InC, and P&O.

After designing the Simulink model for PV curve trace and finding the maximum PV value, we design their controller and converter with the help of the DF algorithm and some research data. In this, each panel is connected to a separate DC-DC converter and computation can be done with present research data. The Simulink model of the MLPE distributed PV system is shown in Figure 12. The monitoring scope is attached with each source current, voltage and duty cycle.

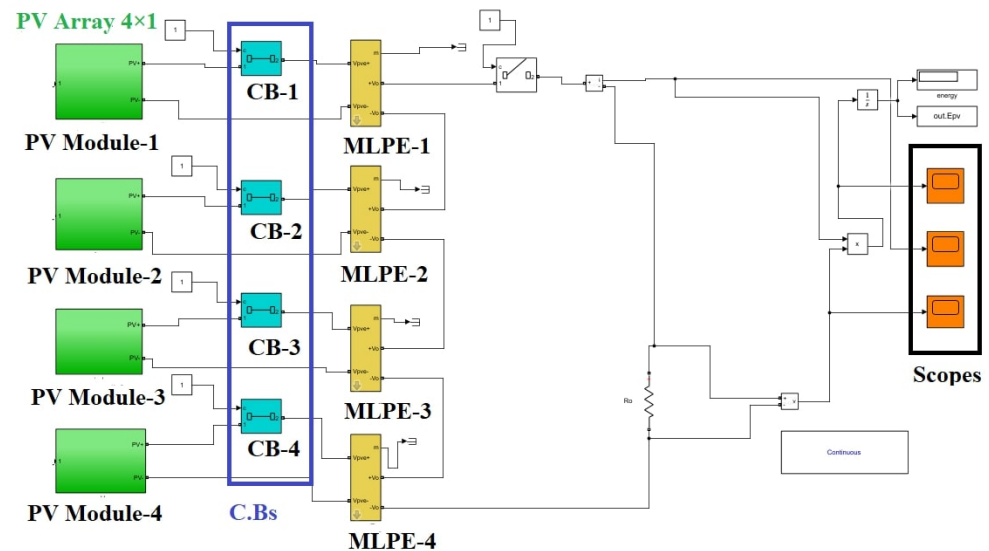


Figure 12. Complete Simulink model of MLPE distributed PV system.

Table 3. P-V and I-V characteristic curves at different irradiance values of MLPE Distributed PV system.

Case	Irradiance S_i (W/m^2)				$Power_{max}$
Case 1 PS1	PV-1:800	PV-2:600	PV-3:400	PV-4:100	528 W
Case 2 PS2	PV-1:800	PV-2:600	PV-3:400	PV-4:400	548 W
Case 3 PS3	PV-1:800	PV-2:800	PV-3:600	PV-4:600	826 W
Case 4 UI	PV-1:800	PV-2:800	PV-3:800	PV-4:800	940 W

5.3. Electrical Code Requirement

By the National Electrical Code (NEC) the main requirement for the system is the rapid shut down. So, to fulfill this requirement by using the breakers in the centralized and distributed Simulink. On the other hand, more safety can be done by using the scope and display panel. So that system becomes more efficient and more reliable by using these safety tools.

6. Results and Discussion

The result can be made with the help of the Matlab Simulink software and Helioscope designing tools. This software helps us to show the efficiency of MLPE and DMPPT systems. So, for the purpose of efficiency, design the two systems such as centralized and DMPPT on the Matlab and Helioscope for the sake of better efficiency and optimized result. The results for these two systems can be made on the uniform and shading conditions.

The first step is to compute Matlab results in order to find the maximum value produced from the solar PV array. The results of different irradiance conditions for centralized and distributed are shown below.

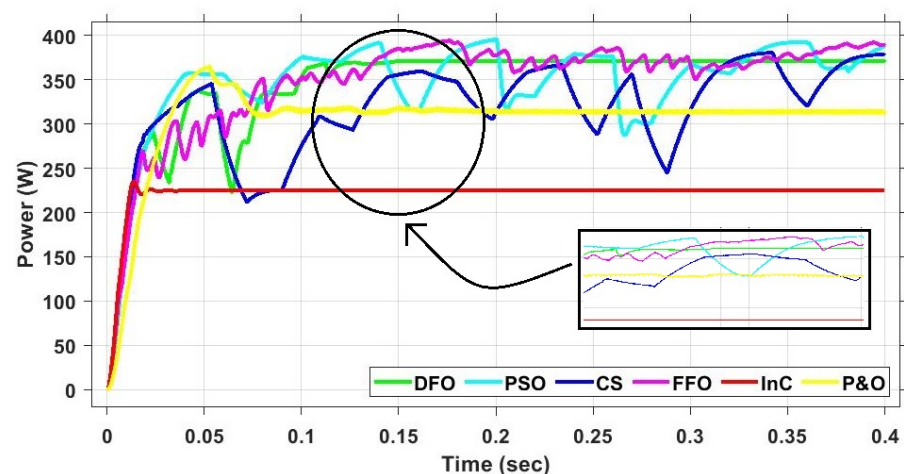
The proposed DF is compared to well-known FFO, CS, InC, P&O, and PSO models. Table 4 compares the findings based on faster tracking, higher tracking performance, ripple elimination, and faster transient response.

Table 4. Comparative analysis of DFO with PSO, CS, FFO, P&O AND InC MPPT algorithm for UI and PS conditions for centralized PV system.

Sr. No	Technique	Case	Convergence Time (s)	Settling Time (s)	Maximum Power (Watt)	Power Tracked (Watt)	Efficiency (%)	GM Detected	Energy
1	DFO	PS1	0.1012	0.1135	375	370.87	98.88	Yes	139.40
		PS2	0.1020	0.1300	494	490.00	99.19	Yes	220.30
		PS3	0.1070	0.1170	740	730.97	98.77	Yes	249.68
		UI	0.1270	0.1166	940	934.00	99.36	Yes	357.00
2	PSO	PS1	0.3351	0.3901	375	370.12	98.69	Yes	139.10
		PS2	0.3156	0.3940	494	479.00	96.96	Yes	200.90
		PS3	0.2931	0.3934	740	710.00	95.94	Yes	249.10
		UI	0.3310	0.3974	940	905.00	96.27	Yes	310.00
3	CS	PS1	0.3015	0.3741	375	369.00	98.40	Yes	127.55
		PS2	0.3512	0.3792	494	487.00	98.50	Yes	218.00
		PS3	0.2510	0.3651	740	725.00	97.97	Yes	247.00
		UI	0.2560	0.3531	940	930.00	98.93	Yes	275.00
4	FFO	PS1	0.2995	0.3993	375	370.25	98.73	Yes	138.40
		PS2	0.1120	0.1365	494	475.00	96.15	Yes	219.10
		PS3	0.2102	0.2902	740	728.00	98.37	Yes	248.50
		UI	0.2013	0.2501	940	910.00	96.80	Yes	347.00
5	P&O	PS1	0.3520	0.4000	375	314.00	93.73	No	123.32
		PS2	0.3651	0.3990	494	410.00	82.99	No	196.00
		PS3	0.3800	0.4000	740	650.00	87.83	No	230.00
		UI	0.3500	0.3996	940	790.00	84.04	No	305.00
6	InC	PS1	0.0101	0.0123	375	224.00	59.73	No	089.44
		PS2	0.0110	0.0125	494	390.00	78.94	No	158.00
		PS3	0.0019	0.0129	740	552.00	74.59	No	162.62
		UI	0.2950	0.3210	940	670.00	71.27	No	290.00

6.1. Case 1 PS1 for Centralized PV System

In the Simulink model of the centralized PV system, examine the different algorithms, which can be compared on different irradiance levels. The simulation is performed on the four panels array. The PV array is connected to a single DC-DC converter. Different irradiance cases are shown below. The power, current and voltage are shown in Figures 13–15, respectively. This will be discussed with respect to the comparison of different algorithms such as DF, PSO, FFO, CS, InC, and P&O. Case 1 shows that all panels have different irradiances of 800, 600, 400, and 100.

**Figure 13.** PS1 power comparison between all algorithms for centralized PV system.

In CS, the maximum power achieved is 522 W and the total energy of 127.55 J with a settling time of 0.3741 s, which is higher than the purposed algorithm. In the Dragon fly algorithm, the maximum power of 525 W is achieved with the energy of 139.4 J having a settling time of 0.1135 s. In the FFO algorithm, the maximum power of 523 W is achieved with the energy of 138.48 with a settling time of 0.3993 s, much higher than other algorithms. PSO tracks the maximum power of 520 W having achieved energy of 139.1 J with the settling time of 0.3901 s. It is followed by InC 367 W, 89.4 J, with a settling time of 0.0123 s, and P&O 462 W, 123.32 J with a settling time of 0.4 s.

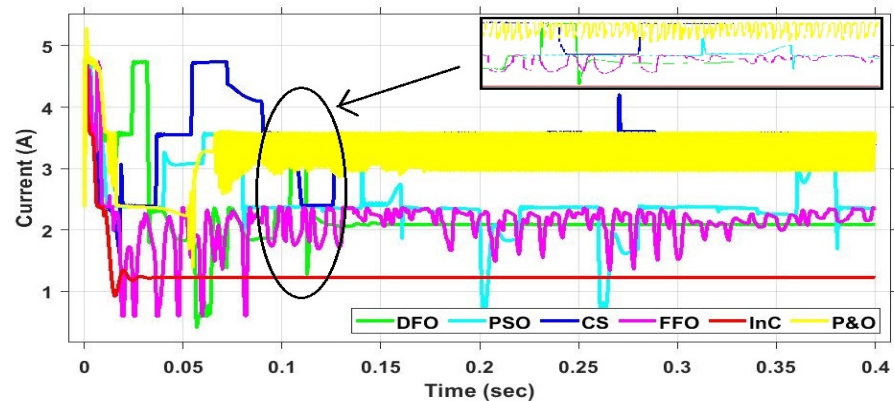


Figure 14. PS1 current comparison between all algorithms for centralized PV system.

The FFO is responsible for the surge oscillations, as shown in the high magnification view. P&O's scaling factor is tuned for quick tracking and minimal vibrations. Dependent on the $\frac{\Delta P}{\Delta d}$ condition, the step size Δd is the fractional change in the current operating point of P&O. Power is lost as a result of the continual disturbances. Overall in the algorithm, the dragon fly shows better results and settling time as compared to other algorithms. P&O and InC cannot achieve the global maximum and have low tracking power. However, the dragon fly has higher power as compare to other algorithms and it has good settling and transient time. DF out do not contain any oscillation in their output, hence there is no power loss.

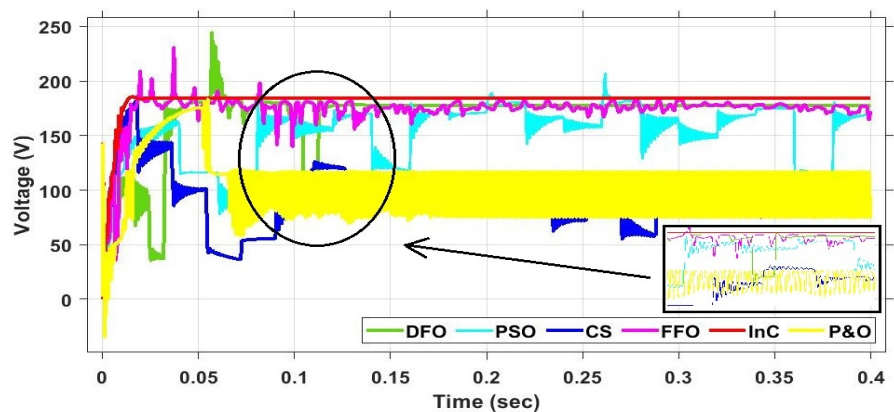


Figure 15. PS1 voltage comparison between all algorithms for centralized PV system.

The average power achieved by Dragon Fly, CS, PSO, FFO, InC, and P&O is 525, 522, 520, 523, 367, and 462 W, respectively. So, from the power, it is concluded that $DF > FFO > CS > PSO > InC > P\&O$. Under quickly fluctuating irradiance, DF is durable and extremely efficient at tracking and re-tracking MPP. Two variables, tracking time (TT) and settling time (ST), are used to assess the durability of alternative methods (ST). The tracking time is calculated from the moment of initiation until the time when MPP is reached. The settling

time refers to the amount of time it takes for particles to settle at MPP without oscillating. Table 4 shows the TT and ST among all involved approaches.

6.2. Case 2 PS2 for Centralized PV System

In the Simulink model of the centralized PV system, different algorithms are considered, which can be compared on different irradiance levels. As PV array is connected to a single DC-DC converter. Different irradiance cases are shown below. The power, current and voltage are given in Figures 16–18 correspondingly. This will be discussed with respect to the comparison of different algorithms such as DF, PSO, FFO, CS, InC, and P&O.

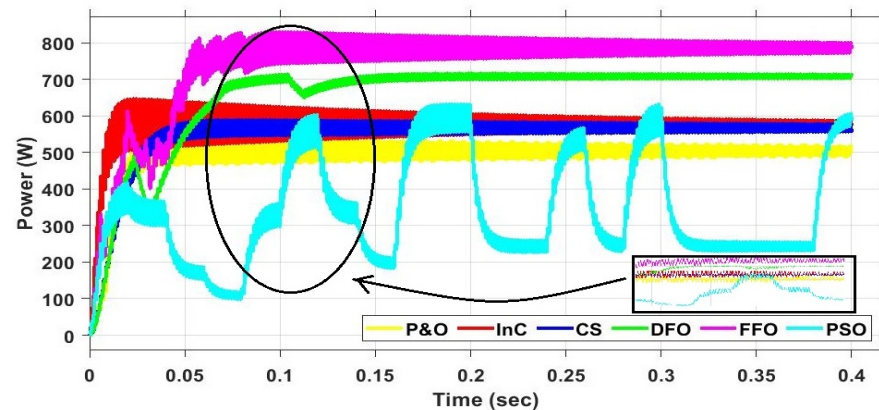


Figure 16. PS2 power comparison between all algorithms for centralized PV system.

Case 2 shows that all panels have different irradiances, 800, 600, 400, and 400. In CS search, the maximum power achieved is 540 W and a total energy of 218 J with a settling time of 0.3792 s, which is higher than a purposed algorithm. In the DF algorithm, the maximum power of 545 W is achieved with the energy 220.3 joule having a settling time of 0.1300 s. In the FFO algorithm, the maximum power of 542 W is achieved with the energy of 219.1 with a settling time of 0.1365 s. PSO tracks the maximum power of 543 W having energy achieved of 200.9 J with the settling time of 0.394 s pretty high than another algorithm. It is followed by InC 400 W, 158 J, with a settling time of 0.0125 s, and P&O 490 W, 196 J with a settling time of 0.034 s. The high magnification picture shows that the PSO causes the surge oscillations, which can be reduced by changing the swarm placement and position. The continuous oscillations cause power loss. Over the algorithm, Dragon Fly shows better results and settling time as compared to other algorithms. P&O and InC cannot achieve the global maximum and have low tracking power. However, the dragon fly has higher power as compare as compared to other algorithms and it has good settling and transient time. DF out don't contain any oscillation in their output hence there is no power loss.

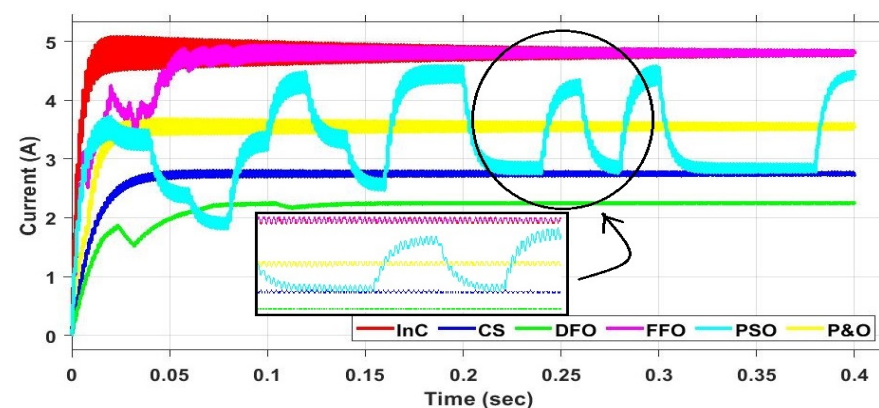


Figure 17. PS2 current comparison between all algorithms for centralized PV system.

Dragon Fly, CS, PSO, FFO, InC, and P&O have an average power of 545, 540, 543, 542, 400, and 490 W, respectively, $DF > PSO > FFO > CS > InC > P\&O$. Under quickly fluctuating irradiance, DF is durable and extremely efficient at tracking and re-tracking MPP. Two variables, TT and ST, are used to assess the durability of competing techniques. The tracking time is calculated from the moment of initiation till the time when MPP is achieved. The ST refers to the amount of time it takes for particles to settle at MPP without oscillating. Table 4 shows the TT and ST of all related approaches. TT can be neglected in InC and P&O even though it is trapped at LM and unable to locate GM.

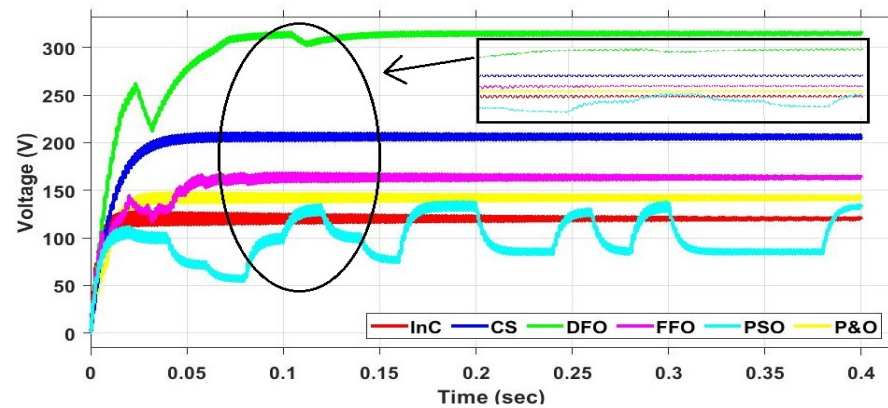


Figure 18. PS2 voltage comparison between all algorithms for centralized PV system.

6.3. Case 3 PS3 for Centralized PV System

This shows that the PV array is connected to two panels that have uniform irradiance and two have 600 irradiances. Different irradiance cases are shown below. The power, current, and voltage are given in Figures 19–21, respectively, and discussed with respect to the comparison of different algorithms such as DF, PSO, FFO, CS, InC, and P&O. Case 3 shows that all panels have different irradiances of 800, 800, 600, and 600, and on this irradiance level as shown in the figure below.

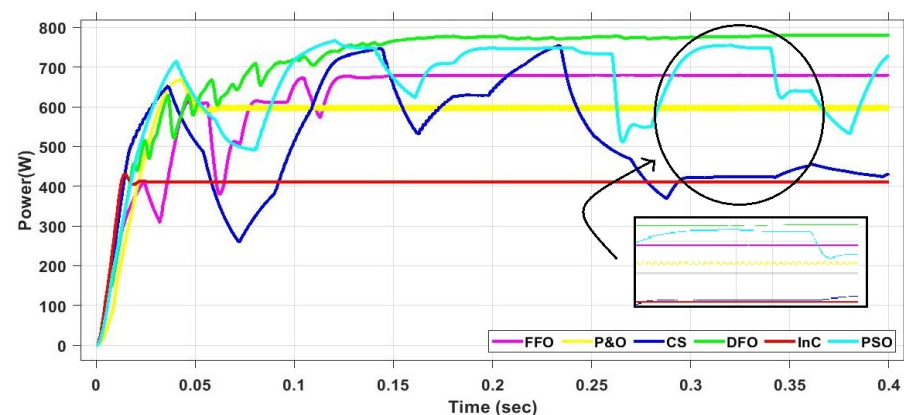


Figure 19. PS3 power comparison between all algorithms for centralized PV system.

Case 3 is another PS case. In this scenario, the PS is modeled with a distorted MPP placement. The array is set up in a 4×1 layout. The GM is located at 826 W. The MPP is biased from the center. On P-V curves, the MPPs are at 486.74 W, with the associated voltage of 105 and 226 V. The study demonstrates that the CS locates GM in 0.3531 s, while the PSO tries to find GM in 0.3974 s with an extracted power of 820 W and the FFO retrieves 815 W. DF enhances the system's ability to inhibit fluctuations even more, and thus its average power is larger than PSO's.

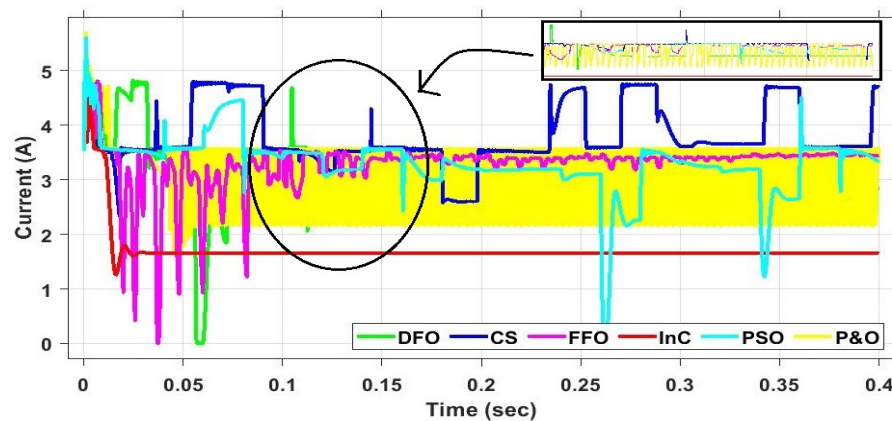


Figure 20. PS3 current comparison between all algorithms for centralized PV system.

The instability greatly diminishes the power, according to the results. As a result, DF is built to reduce steady-state fluctuation at GM. The GM is tracked by CS, DF, FFO, PSO, InC, and P&O in 0.251, 0.107, 0.2102, 0.2931, 0.0019, and 0.380 s, correspondingly, with ST of 0.3651, 0.117, 0.2902, 0.3934, 0.0129, and 0.4000 s. DF has the largest power production at 821.3W, supported by CS 819 W, FFO 815 W, PSO 820 W, InC 660, and P&O 675 W, in that order. The algorithm shows that dragonflies have better results and settling times as compared to other algorithms.

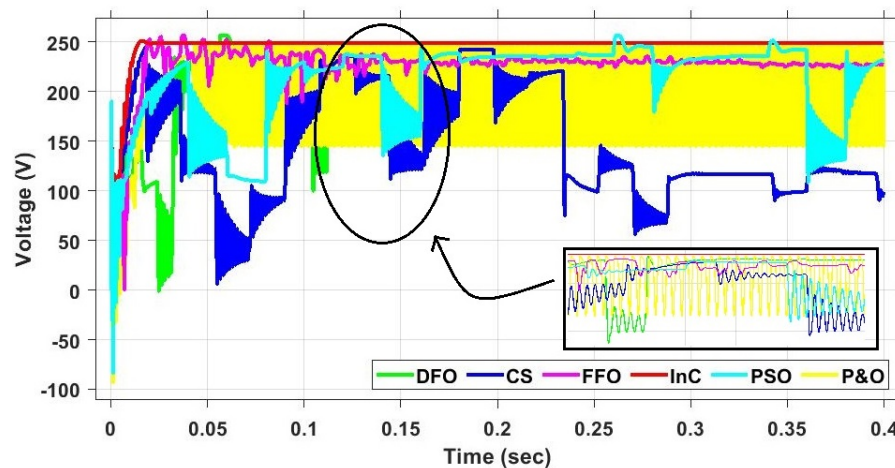


Figure 21. PS3 voltage comparison between all algorithms for centralized PV system.

6.4. Case 4 UI for Centralized PV System

This show that all panels have the same irradiance of 800, 800, 800, and 800 on this irradiance level maximum value of MPPT will be achieved. The power, current and voltage are given in Figures 22–24, respectively.

The uniform irradiance is Case 4. The Uniform MPP location is modeled in this example. The array is set up in a 4×1 layout. The GM is situated at 940 W. The MPP is right from the center. On P-V curves, the MPPs are at and 940 W, with matching voltages of 225 V. The results demonstrate that whereas the CS manages to find GM in 0.3531 s, the PSO detects GM in 0.3974 s with an obtained power of 914 W and the FFO retrieves 915 W. DF enhances the system's ability to inhibit oscillations even more, and its average output powers larger than PSO's.

The oscillation greatly diminishes the power, according to the results. As a result, DF is built to reduce steady-state oscillation at GM. CS, DF, FFO, PSO, InC, and P&O follow the GM in 0.256, 0.127, 0.2013, 0.3331, 0.295, and 0.350 s, respectively, with ST of 0.3531, 0.1366, 0.3974, 0.321, and 0.3996 s. DF has the largest power production (935 W), next by CS (934 W), FFO (915 W), PSO (914 W), InC 685 W, and P&O 766.5 W (DF > CS > FFO > PSO >

P&O > InC). Generally, the algorithm reveals that DF produces superior results and has a shorter ST than other techniques.

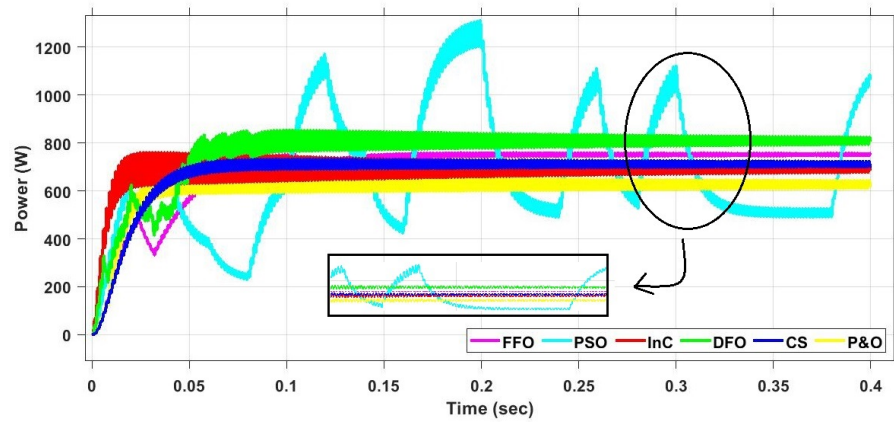


Figure 22. UI power comparison between all algorithms for centralized PV system.

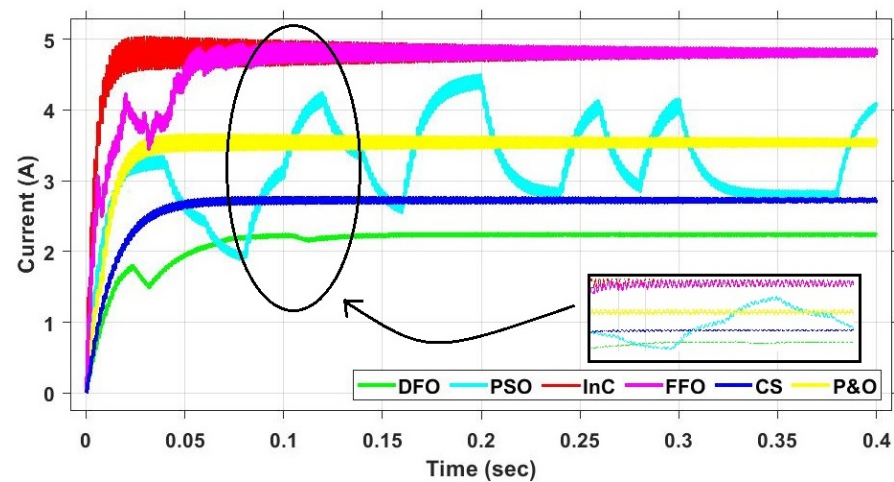


Figure 23. UI current comparison between all algorithms for centralized PV system.

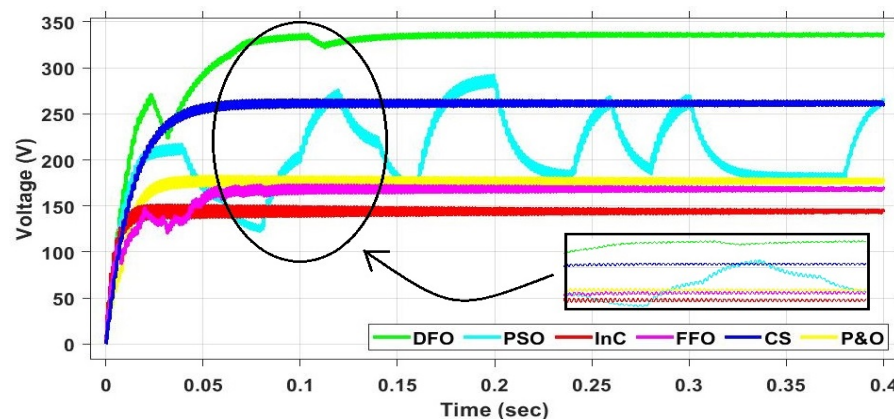


Figure 24. UI voltage comparison between all algorithms for centralized PV system.

6.5. Case 1 PS1 MLPE Distributed PV System

Case 1 shows that all panels have different irradiance and on this irradiance level the MPPT algorithm CS, DF, PSO, FFO InC, and P&O shows different values of current-voltage and power depending on the algorithm mechanism. The distributed PV system computes better efficiency as compared to the centralized PV system we can verify it through Table 5.

Power comparisons of the different algorithms are shown in the Figure 25 and the dragon fly shows the better performance on all of the algorithms.

Table 5. Comparative analysis of DFO with PSO, CS, FFO, P&O AND InC MPPT Algorithm for UI and PS Conditions for MLPE distributed PV system.

Sr. No	Technique	Case	Convergence Time (s)	Settling Time (s)	Maximum Power (Watt)	Power Tracked (Watt)	Efficiency (%)	GM Detected	Energy
1	DFO	PS1	0.0951	0.1140	528	525.00	99.43	Yes	193.05
		PS2	0.0420	0.0670	548	545.00	99.45	Yes	250.04
		PS3	0.1280	0.1660	826	821.30	99.47	Yes	304.50
		UI	0.1010	0.1136	940	935.00	99.46	Yes	358.60
2	PSO	PS1	0.3129	0.3868	528	520.00	98.48	Yes	164.70
		PS2	0.3231	0.3733	548	543.00	99.00	Yes	183.00
		PS3	0.3215	0.3919	826	820.00	99.27	Yes	260.00
		UI	0.3870	0.3627	940	914.00	97.23	Yes	317.00
3	CS	PS1	0.3527	0.3696	528	522.00	98.86	Yes	148.40
		PS2	0.3423	0.3688	548	540.00	98.50	Yes	176.80
		PS3	0.3150	0.3747	826	819.00	99.15	Yes	252.40
		UI	0.1143	0.3886	940	934.00	99.36	Yes	276.30
4	FFO	PS1	0.1519	0.1926	528	523.00	99.05	Yes	159.70
		PS2	0.1057	0.1320	548	542.00	98.90	Yes	235.00
		PS3	0.1952	0.2028	826	815.00	98.66	Yes	265.00
		UI	0.2589	0.3370	940	915.00	97.34	Yes	351.00
5	P&O	PS1	0.0123	0.0200	528	462.00	87.50	No	183.00
		PS2	0.0210	0.0300	548	490.00	89.41	No	188.00
		PS3	0.0120	0.0200	826	675.00	81.71	No	263.00
		UI	0.0250	0.0300	940	766.50	81.50	No	290.00
6	InC	PS1	0.0123	0.0200	528	367.00	69.50	No	145.00
		PS2	0.0210	0.0268	548	400.00	72.99	No	183.00
		PS3	0.0112	0.0145	826	660.00	79.90	No	250.00
		UI	0.0120	0.0150	940	685.00	72.87	No	273.00

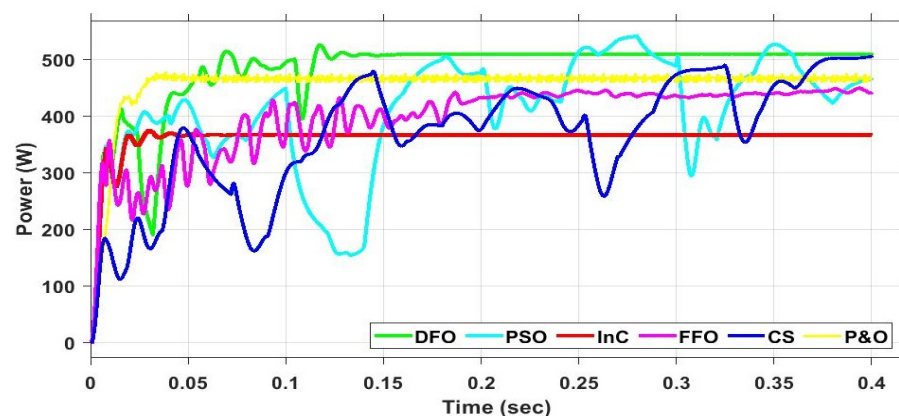


Figure 25. PS1 power comparison between all algorithms for MLPE Distributed PV system.

The CS algorithm shows the maximum power achieved of 522 W with a settling time of 0.3696 s and efficiency of 98.84%, and this helps achieve the GM. The FFO algorithm shows the maximum power of 523 W having a settling time of 0.1926 W. PSO shows the power of 520 W with an efficiency of 98.48%. PSO has higher settling as compared to other algorithms. The current comparison of various algorithms is shown in the Figure 26.

DF has achieved a power of 525 W, having a good settling time compared to other bio-inspired techniques. The other two traditional techniques such as InC and P&O have low power and did not achieve the global maxima peak, but their settling time is very fast.

However, we can't fulfill our desired power. Voltage comparisons are elaborated in the Figure 27.

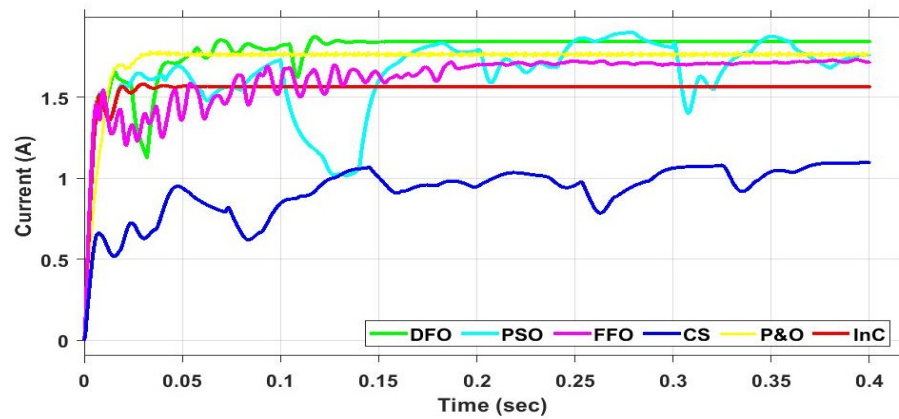


Figure 26. PS1 current comparison between all algorithms for MLPE Distributed PV system.

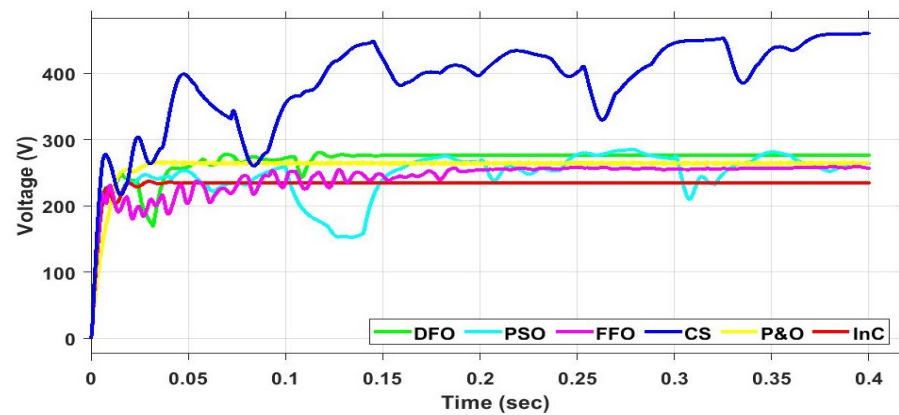


Figure 27. PS1 voltage comparison between all algorithms for MLPE Distributed PV system.

Oscillation in PSO is high, which causes power losses. Hence, DF achieves the global maximum with the Fast settling time and transient response, and there is no oscillation in the output, so there is no power loss.

6.6. Case 2 PS2 MLPE Distributed PV System

In case 2, the irradiance discussed as two panels have the same 800 and two have the same 600 irradiances. The power, current and voltage are described in Figures 28–30, respectively.

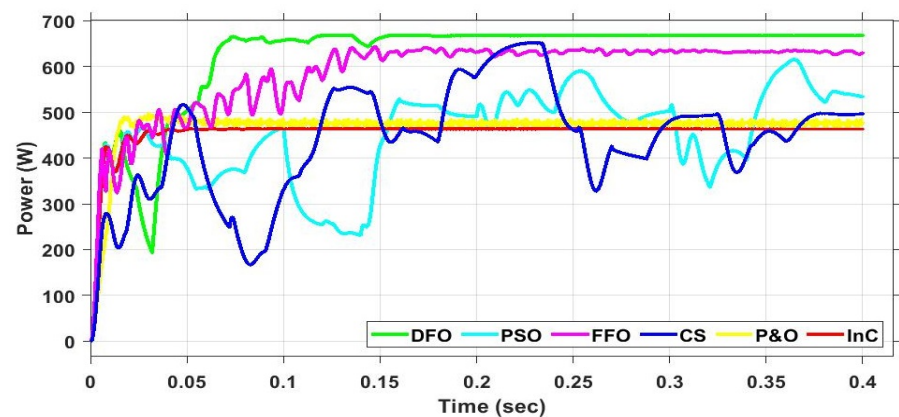


Figure 28. PS2 power comparison between all algorithms for MLPE Distributed PV system.

In CS search, the maximum power achieved is 540 W and the total energy of 176.8 J with a settling time of 0.3423 s and the global maximum is achieved. In the Dragon fly algorithm, the maximum power of 545 W is achieved with the energy 250.04 J having a settling time of 0.042 s. In the FFO algorithm, the maximum power of 542 W is achieved with the energy of 235 with a settling time of 0.1057 s. PSO track the maximum power of 543 W having energy achieved of 183 J with the settling time of 0.3231 s pretty and GM is achieved. It is followed by InC 400 W, 183 J, with a settling time of 0.021 s, and P&O 490 W, 188 J with a settling time of 0.021 s.

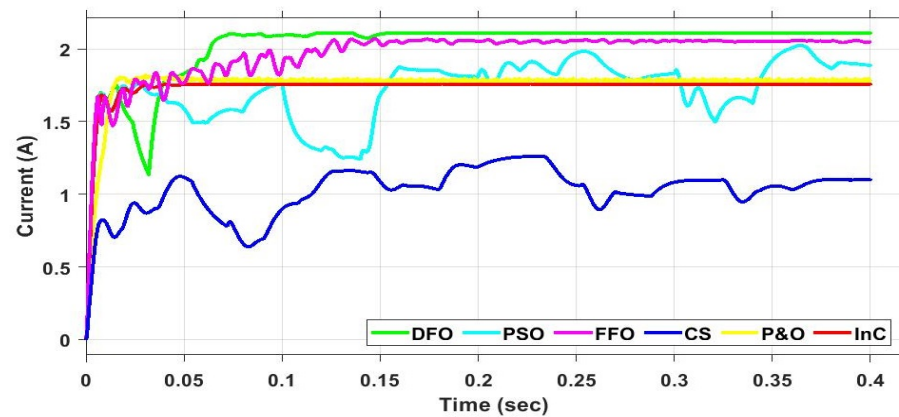


Figure 29. PS2 current comparison between all algorithms for MLPE Distributed PV system.

The high magnification picture shows that the PSO and CS create surge oscillations, which can be reduced with better positioning and repetition. The continuous oscillations cause power loss. Over the algorithm, Dragon Fly shows better results and settling time as compared to other algorithms.

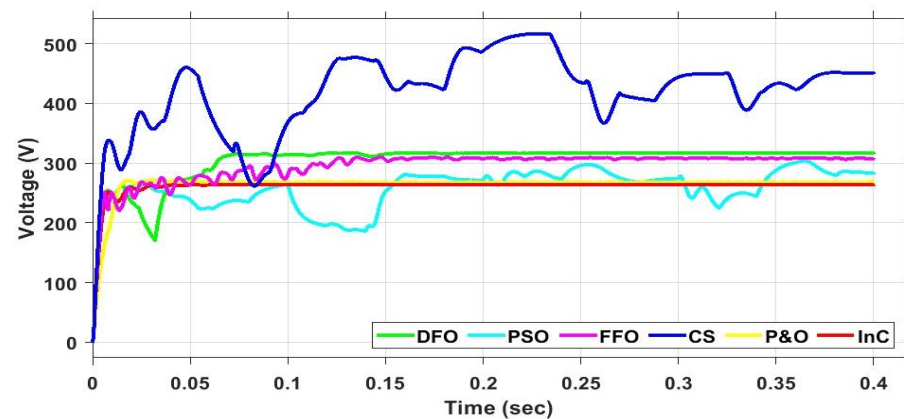


Figure 30. PS2 voltage comparison between all algorithms for MLPE Distributed PV system.

DFs, PSO, PSO, CS, InC, and P&O have an average output power of 545, 540, 543, 542, 400, and 490 W, accordingly. Under quickly fluctuating irradiance, DF is durable and extremely efficient at tracking and re-tracking MPP. Two variables, TT and ST, are used to assess the durability of competing techniques. The tracking time is calculated from the moment of initiation until the time when MPP is reached. The ST refers to the amount of time it takes for the particulate to settle at MPP without fluctuating. Table 5 shows the TT and ST of all related approaches. TT can be ignored in InC and P&O, so it is trapped at LM and unable to find GM. The voltage, power, and current are depicted in the diagram below.

6.7. Case 3 PS3 MLPE Distributed PV System

Case 3 shows that all panels have different irradiance, and on this irradiance level the MPPT algorithm, CS, DF, PSO, FFO InC, and P&O show different values of current, voltage,

and power depending on the algorithm mechanism. The distributed PV system computes better efficiency, as compared to the centralized PV system, we can verify it through Table 5. The power comparison of various techniques is presented in the Figure 31. Thus, the dragon fly shows better performance on all of the algorithms. The CS algorithm shows the maximum power achieved of 819 W with a settling time of 0.3747 s and efficiency of 99.15%, and this help achieve the global maximum. The FFO algorithm shows the maximum power of 815 W having a settling time of 0.2020 s. PSO shows the power of 820W with an efficiency of 99.27%. Current and voltages comparison are given in Figures 32 and 33.

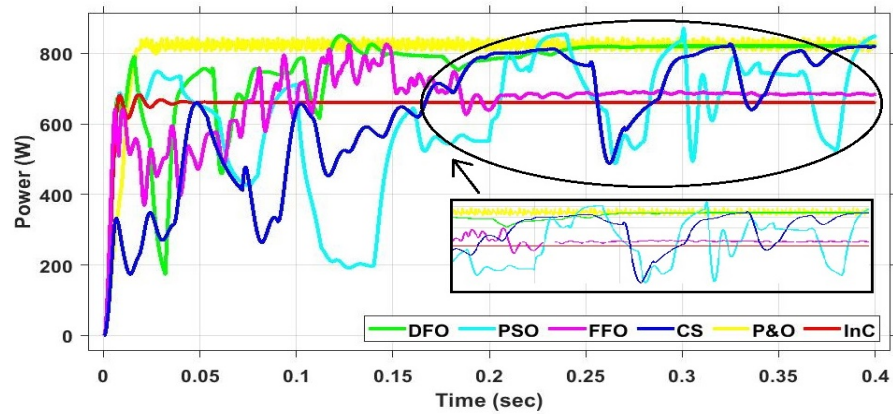


Figure 31. PS3 power comparison between all algorithms for MLPE Distributed PV system.

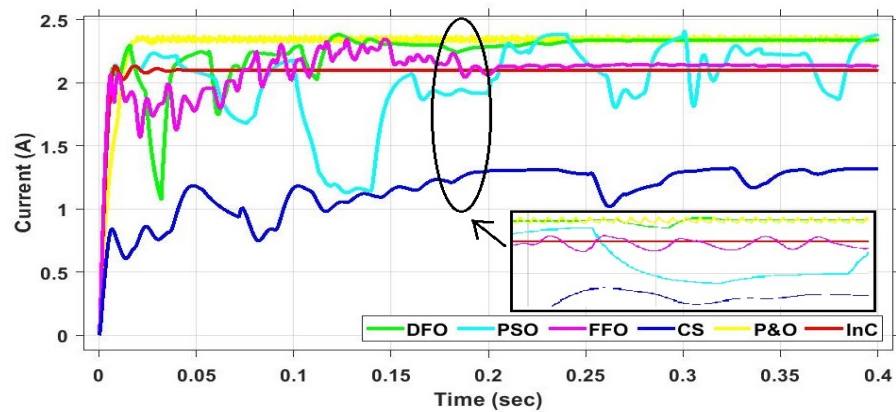


Figure 32. PS3 current comparison between all algorithms for MLPE Distributed PV system.

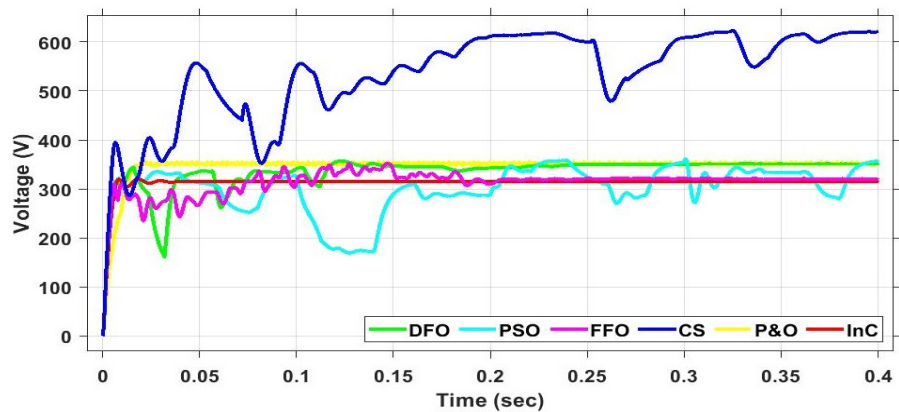


Figure 33. PS3 Voltage comparison between all algorithms for MLPE Distributed PV system.

6.8. Case 4 UI MLPE Distributed PV System

In case 4, the irradiance is discussed, as all panels have the same 800 irradiances. The power, current and voltage are described in Figures 34–36, respectively. In CS search, the maximum power achieved is 934 W and the total energy of 273.6 J with a settling time of 0.3886 s and the global maximum is achieved. In the Dragon fly algorithm, the maximum power of 935 W is achieved with the energy 358.6 J having a settling time of 0.1136 s. In the FFO algorithm, the maximum power of 915 W is achieved with the energy of 351 J with a settling time of 0.337 s. PSO track the maximum power of 914W having achieved an energy of 317 J with the settling time of 0.3627 s pretty and GM is achieved. It is followed by InC 685 W, 273 J, with a settling time of 0.012 s, and P&O 766.5 W, 290 J with a settling time of 0.025 s.

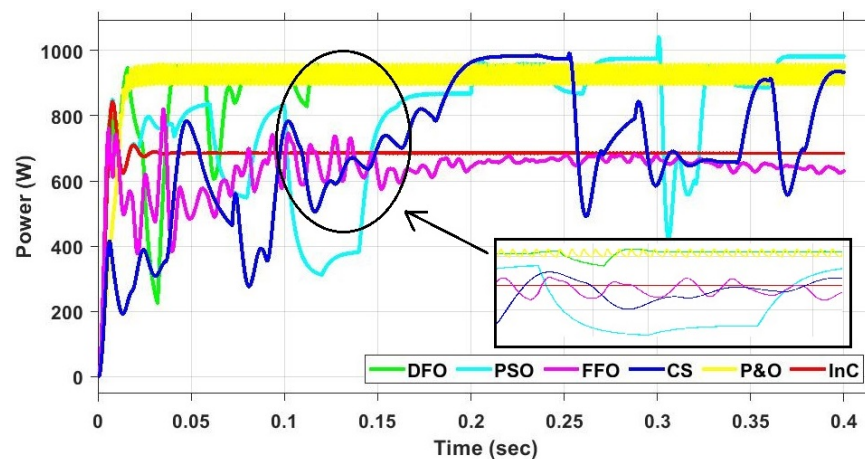


Figure 34. UI power comparison between all algorithms for MLPE Distributed PV system.

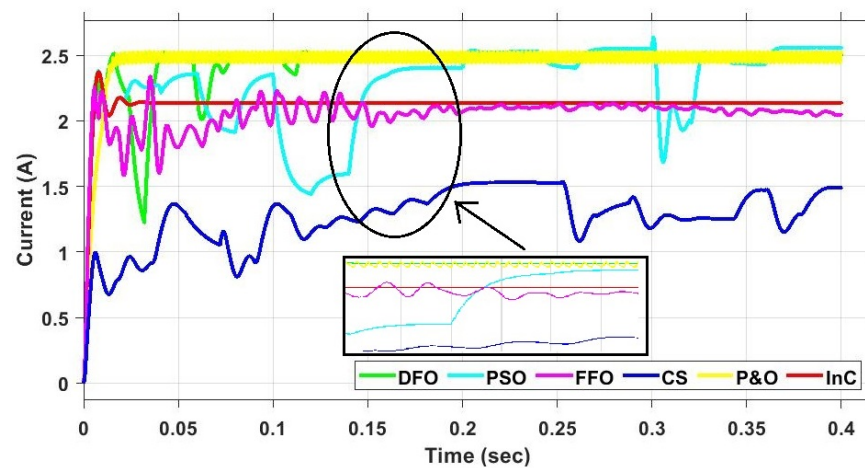


Figure 35. UI current comparison between all algorithms for MLPE Distributed PV system.

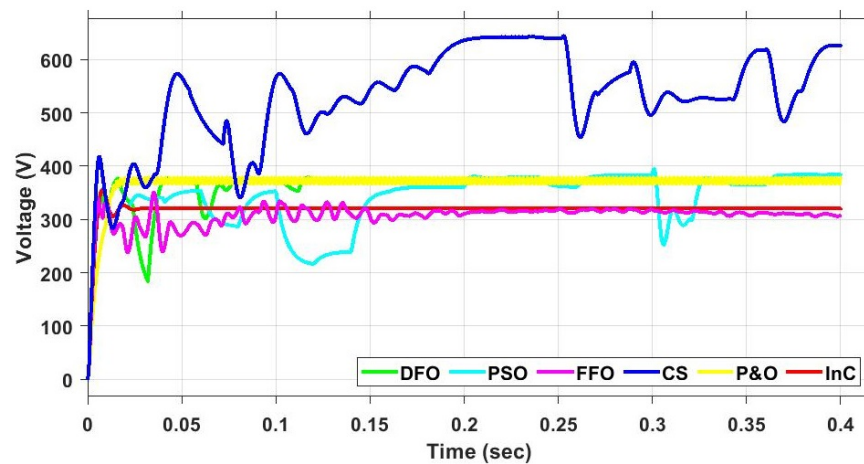


Figure 36. UI voltage comparison between all algorithms for MLPE Distributed PV system.

The surge oscillations are generated by the PSO and CS, which can be reduced with the right position and placement, as well as additional repetition. The continuous oscillations cause power loss. Of all the algorithms, dragon fly shows better results and settling time as compared to other algorithms.

The average power achieved by Dragon fly, CS, PSO, FFO, InC, and P&O is 935, 934, 914, 915, 685, and 766.5 W, respectively, DF > CS > FFO > PSO > P&O > InC.

7. Efficiency of PV System and Analysis

Due to the varying nature of PV systems, MPPT algorithms are required to obtain the maximum power from PV modules. In a PV system, the PV system input impedance of the DC to DC converters is dynamically varied by these algorithms to achieve maximum energy transmission. Power converters, which are subjected to frequent fluctuation in the operating point, will have the greatest influence on the efficiency of the solar system. The IEC 61683:2000 standard specifies the fundamental processes for assessing efficiency. This key parameter illustrates the efficiency of a converter at varying operating points and times. The equations of the overall weighted efficiency are given below as follows:

$$\eta_w = \frac{\sum_{(i=1)}^k P_{out,i} \times t_i}{\sum_{(i=1)}^k P_{in,i} \times t_i} \tag{9}$$

$$= \frac{P_{out,1} \times t_1 \times \eta_1 + P_{out,2} \times t_2 \times \eta_2 + \dots + P_{out,n} \times t_n \times \eta_n}{P_{in,1} \times t_1 \times \eta_1 + P_{in,2} \times t_2 \times \eta_2 + \dots + P_{in,n} \times t_n \times \eta_n}$$

$$\eta_w = \sum_{(i=1)}^k K_i \times \eta_i \tag{10}$$

$$= K_1 \times \eta_1 + K_2 \times \eta_2 + \dots + K_n \times \eta_n$$

here, $P_{out,i}$, $P_{in,i}$, t_i , K_i and η_i show the output power, input power, operating time, weighting constant and efficiency of the PV system correspondingly at i th power range. The value of K_i is given below:

$$K_i = \frac{P_{out,i} \times t_i}{P_{in,i} \times t_i} \tag{11}$$

where $\sum_{(i=1)}^k K_i = 1$. For weighing constant, K_i is the time span that a converter runs with granted power. So, it is directly related to the time that sunlight reaches the PV modules in PV systems.

Under quickly fluctuating irradiance, DF is durable and extremely efficient at tracking and re-tracking MPP. Two variables, TT and ST, are used to assess the sturdiness of competing approaches. The TT is calculated from the moment of initiation until the time when MPP is reached. The ST refers to the amount of time it takes for particles to settle at

MPP without oscillating. Table 5 shows the TT and ST of all related approaches. TT can be ignored in InC and P&O because it is locked at LM and unable to locate GM. DF algorithm has a faster settling time and has no oscillation in their output, and there is no power loss. The voltage, and power, are currently shown in the figure below.

PSO has higher settling as compared to other algorithms. DFO has a lesser settling time compared to other bio-inspired techniques $DF > PSO > CS > FFO > P\&O > InC$. The other two traditional techniques such as InC and P&O have low power and did not achieve the global maxima peak, but their settling time is very fast. However, we cannot fulfill our desired power. And oscillation in PSO is high which causes the power losses. Hence, DF achieves the global maximum with the Fast settling time and transient response, and there is no oscillation in the output so there is no power loss.

8. Comparative Analysis of MLPE Distributed and Centralized PV System

In the end, the result is concluded with the help of comparison Tables 4 and 5 on the PV curve, which are shown below. The result is based on different irradiance and measurement conditions. The comparative analysis is based on the discussion of the result of a distributed and centralized PV system. These two topologies can be based on the comparative results with the different algorithm such as CS, DF, FFO, PSO, InC, and P&O. The centralized PV system contain a single DC-DC converter, which is a boost converter for all the four panels and all algorithm can be implemented in the place of the MPPT controller. However, in the distributed PV system, all the panels have their own DC-DC converter and all converters computed results on the different algorithms.

Different cases can be made on shading and UI for both centralized and distributed systems. Case 1 considers the PS on all the panel 800, 600, 400, and 100. Case 2 is the partial shading condition of 800, 600, 400, and 400. Case 3 was made on the 800, 600, 600, and 800 shading conditions. Case 4 is the uniform irradiance condition. These four cases compare the efficiency of the centralized and distributed PV system, which depends on the computed algorithm. The actual and tracking power can also be observed for the sake of efficiency. This can also be seen when the algorithm achieves the global maximum at very fast ST and TT.

The energy of DMPPT > Centralized for all the cases of energy in CS, DF, FFO, PSO, INC, and P&O. It is also seen that the oscillation in case of DMPPT < Centralized system, and also their time of stability is minimum and fast. The convergence time of DMPPT < Centralized PV system. The comparison is also made on the basis of current (I) and Voltage (V) in the DMPPT and centralized system. It is also shown that the current for the case of DMPPT > centralized, the current in DMPPT $ST < ST$ for centralized, and also the converter for DMPPT current stability is faster than the convergence for the centralized PV system. The Voltage comparison is also made and found the voltage in the case of DMMPT > Centralized system. The main aim of the result is to compute the Power and its efficiency. The efficiency for the DMPPT > then the efficiency of the centralized PV system. $CT > CT$ for the centralized system.

It is shown from the results that distributed PV systems and centralized show very satisfactory results. The MLPE distributed system always shows higher efficiency than the centralized PV system in all four cases. The ST and CT distributed also have better than the centralized PV system. The global peak finding time of the distributed PV system is better than the centralized PV system. The energy can also be calculated by the integration of the power for both centralized and distributed systems. It is shown from the results that the energy of the distribution is higher than the centralized PV system for all cases.

9. Helioscope Results

For further discussion and verification of results, the system can be tested with the Helioscope software. In this software, different companies can be compared such as Enphases, SMA, Solar Edge, Huawei, and Tigo. These companies can be compared with respect to the centralized and MLPE/power optimizer under-tested with the irradiance conditions, and a satisfying result can be received from this software. This result can be made on a 0.25 MW system with simple string inverters and MLPE inverters and converters.

Different cases are examined with respect to companies' inverters and converters. For this purpose, two-field segments depend on the area having tilt 0 and azimuth 180. The Canadian solar panels are used for testing and computing the results.

9.1. Tigo Solar System

In order to test the Tigo optimizer, a 240 kW system having 431 modules, 431 optimizers, and 12 inverters of Huawei were used for synchronization. The losses graph with respect to different losses based on the partial shading and uniform is shown in Figure 37.

Case 1 presents uniform irradiance and shows the different losses like shading 0.0%, reflection 3.9%, Soiling 2.0%, Irradiance 0.5%, AC system 0.5%, and inverter 1.7%, clipping 0.0% wiring 0.6%, optimizers 0.2%, Mismatch 0.4% and Temperature 6.5%.

Figure 37 shows the 25% shading condition as case 2 losses to cover such as shading 0.0%, reflection 3.9%, Soiling 2.0%, Irradiance 0.6%, AC system 0.5%, and inverter 1.7%, wiring 0.7%, optimizers 0.2%, Mismatch 7.0% and Temperature 6.8%.

In case 3, the losses made on 50% shading and losses are discussed in Figure 37 as shading 0.0%, reflection 3.9%, Soiling 2.0%, Irradiance 0.6%, AC system 0.5%, and inverter 1.7%, wiring 0.7%, optimizers 0.2%, Mismatch 7.0%, and Temperature 6.8%.

In case 4, the losses made on 65% shading and losses are discussed in Figure 37 as shading 0.0%, reflection 3.9%, Soiling 2.0%, Irradiance 0.8%, AC system 0.5%, and inverter 1.7%, wiring 0.8%, optimizers 0.2%, Mismatch 14.3%, and Temperature 7.7%.

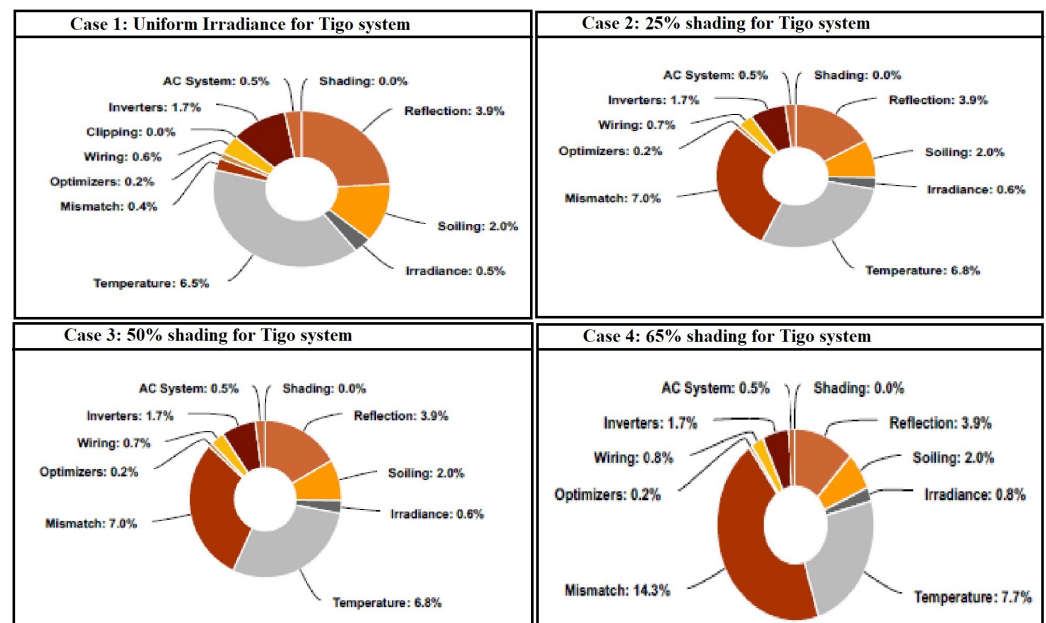


Figure 37. Results of various losses of Tigo solar system on different shading conditions using Helioscope.

Energy production on a per monthly bases is described by the level of irradiance. Figure 38 shows the uniform irradiance level with the annual production of 355.8 MW having a performance ratio of 84.6% with maximum production in June and minimum production in December with 12 combining poles and 2 field segments. On the other hand, Figure 38 shows case 2 of the 25% shading with the annual production of 330.7 MW having a performance ratio of 78.6 with maximum production in June and minimum production in December with 12 combining poles and 2 field segments. In Figure 38, case 3 show the 50% irradiance with the annual production of 330.7 MW having a performance ratio of 78.6% with maximum production in June and minimum production in December with 12 combining poles and 2 field segments. In Figure 38, case 4 shows the 65% shading with the annual production of 302.4 MW having a performance ratio of 71.9% with maximum

production in June and minimum production in December with 12 combining poles and 2 field segments.

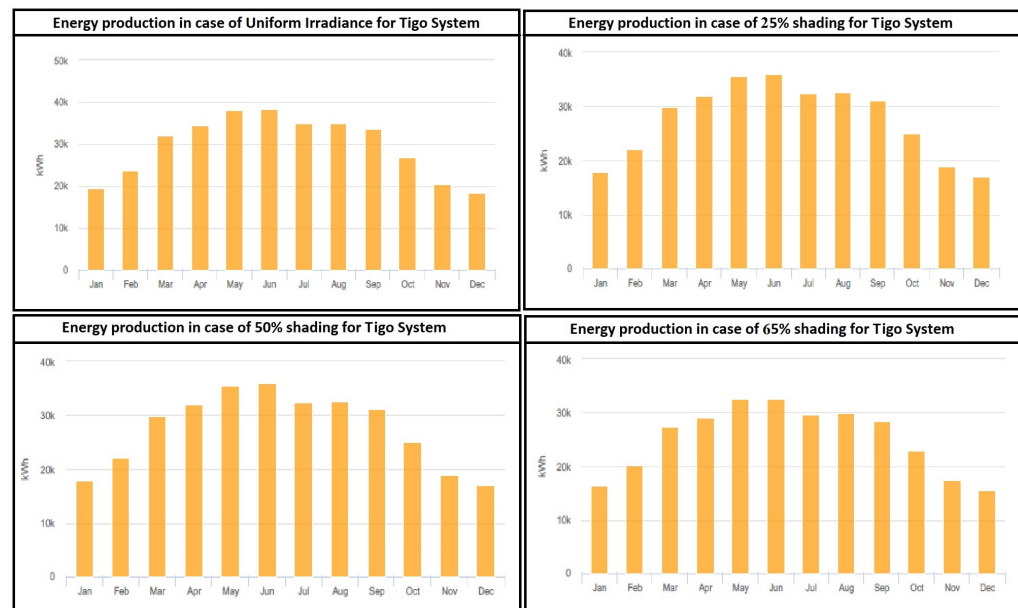


Figure 38. Results of energy production of Tigo solar system on different shading conditions using Helioscope.

9.2. Huawei Solar System

In order to test the Huawei optimizer, a 239 kW system having 545 modules, 545 optimizers and 12 inverters of Huawei used for synchronization. The losses graph with respect to different losses is shown in figure below. Figure 39 shows case 1 for uniform different losses like shading 0.0%, reflection 3.9%, Soiling 2.0%, Irradiance 0.5%, AC system 0.5%, and inverter 1.7%, clipping 0.0% wiring 0.1%, optimizers 1.0%, Mismatch 0.0% and temperature 6.5%. In Figure 39, case 2 shows the 25% shading condition as losses to cover such as shading 0.0%, reflection 3.9%, Soiling 2.0%, Irradiance 0.6%, AC system 0.5%, and inverter 1.7%, wiring 0.2%, optimizers 1.0%, Mismatch 0.0%, and temperature 6.8%. In case 3, the losses made on 50% shading and the losses have been discussed in Figure 39 as shading 0.0%, reflection 3.9%, Soiling 2.0%, Irradiance 0.6%, AC system 0.5%, and inverter 1.7%, wiring 0.2%, optimizers 1.0%, Mismatch 0.0% and temperature 6.8%. In case 4, the losses made on 65% shading and the losses have been discussed in Figure 39 as shading 0.0%, reflection 3.9%, Soiling 2.0%, Irradiance 0.7%, AC system 0.5%, and inverter 1.7%, wiring 0.2%, optimizers 2.7%, Mismatch 14.3% and temperature 7.8%.

Energy products on per monthly bases describe with the level of irradiance. Figure 40 shows the uniform irradiance level with the annual production of 349.8 MWh having a performance ratio of 84.7% with maximum production in June and minimum production in December with 12 combining poles and 2 field segments. In the meantime, Figure 40 elaborates the 25% shading with the annual production of 348 MWh having a performance ratio of 84.3%, with maximum production in June and minimum production in December with 12 combining poles and 2 field segments. Case 3 presents the 50% shading with the annual production of 345 MWh having a performance ratio of 84.1%, with maximum production in June and minimum production in December with 12 combining poles and 2 field segments. Case 4 shows the 65% irradiance with the annual production of 339.6 MWh having a performance ratio of 82.3%, with maximum production in June and minimum production in December with 12 combining poles and 2 field segments.

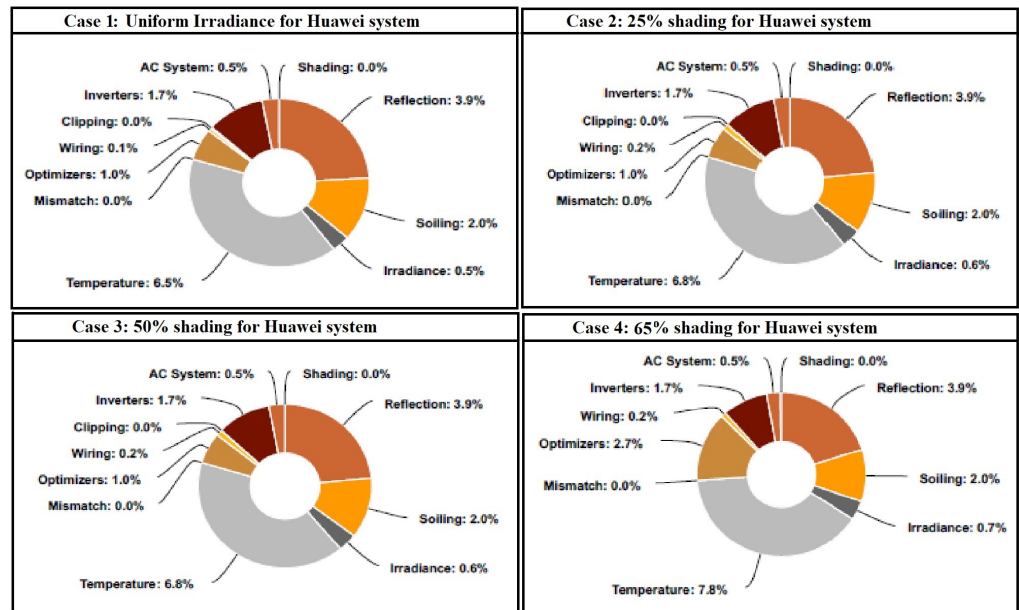


Figure 39. Results of various losses of Huawei Solar system on different shading conditions using Helioscope.

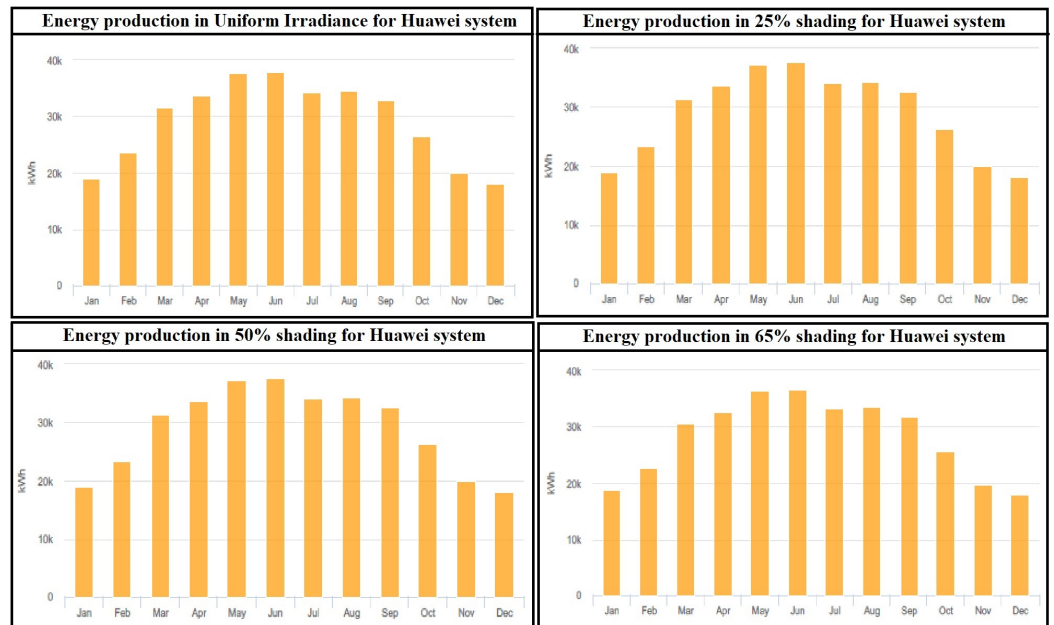


Figure 40. Results of energy production of Huawei Solar system on different shading conditions using Helioscope.

9.3. Solar Edge System

In order to test the solar edge optimizer, a 244 kW system having 431 modules, 431 optimizers, and 5 inverters of the solar edge were used for synchronization. The losses graph with respect to different losses is shown in the figures below different cases have been made on the level of irradiance 4 cases can be made on partial shading and uniform irradiance. Case 1 shows the uniform irradiance having losses can be described as shading losses will be 0.0%, reflection losses are 3.9%, soiling 2.0%, irradiance losses in case of uniform is 0.5% temperature losses will be 6.5% according to the graph Mismatch losses can be 0%, clipping losses 0.1%, wiring 0.1%, Optimizer 1.4%, Inverters 2.0%, AC system 0.5% uniform irradiance losses shown in the Figure 41. In case 2, 25% shading can be considered for the result, and their losses are as follows: shading losses will be 0.0%,

reflection losses are 3.9%, soiling 2.0%, irradiance losses in case 2 are 0.6% temperature losses will be 6.8% according to the graph, Mismatch losses can be 0%, clipping losses 0.0%, wiring 0.2%, Inverters 2.0%, optimizer 1.5%, and AC system 0.5% are expressed in Figure 41. Additionally, 50% shading can be considered for the result, and the losses are as follows: shading losses will be 0.0%, reflection losses are 3.9%, soiling 2.0%, irradiance losses in case 3 are 0.6% temperature losses will be 6.8% according to the graph, Mismatch losses can be 0%, clipping losses 0.0%, wiring 0.2%, Inverters 2.0%, optimizer 1.5%, and AC system 0.5% are presented in case 3. While in case 4, 65% shading can be assumed for the result, and their losses are as follows: shading losses will be 0.0%, reflection losses are 3.9%, soiling 2.0%, irradiance losses in case 4 are 0.8%, temperature losses will be 6.8% according to the graph, mismatch losses can be 0%, clipping losses 0.0%, wiring 0.3%, Inverters 2.0%, optimizer 4.0%, and AC system 0.5% are shown in the Figure 41.

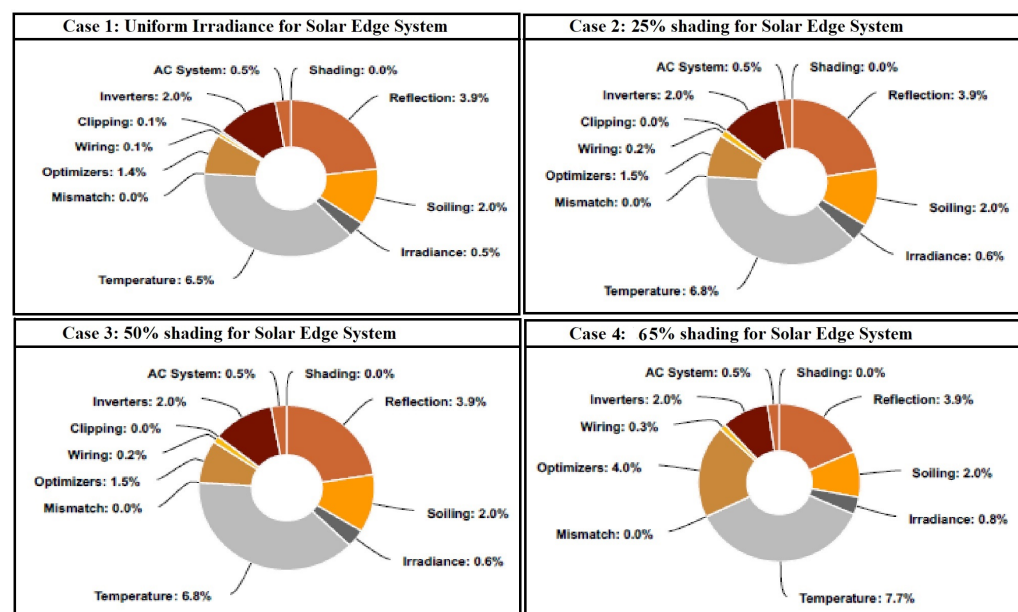


Figure 41. Results of various losses of Solar edge system on different shading conditions using Helioscope.

Energy production per month and year bases are described with the level of irradiance. Additionally, the performance ratio on the basis of production can also be discussed with the help of different irradiance cases. Case 1 shows the uniform irradiance having a performance ratio of 84% with an annual production of 353.5 MWh with two field segments with maximum production in June and minimum production in January. The production graph for the uniform irradiance is shown in the Figure 42 below. Case 2 presents the 25% shading having a performance ratio of 83.8% with an annual production of 352.6 MWh with two field segments with maximum production in June and minimum production in January. Case 3 describes the 50% shading having a performance ratio of 83.6% with an annual production of 351.6 MWh with two field segments with maximum production in June and minimum production in January. Case 4 illustrates the 65% shading having a performance ratio of 80.8% with an annual production of 339.8 MWh with two field segments with maximum production in June and minimum production in January.

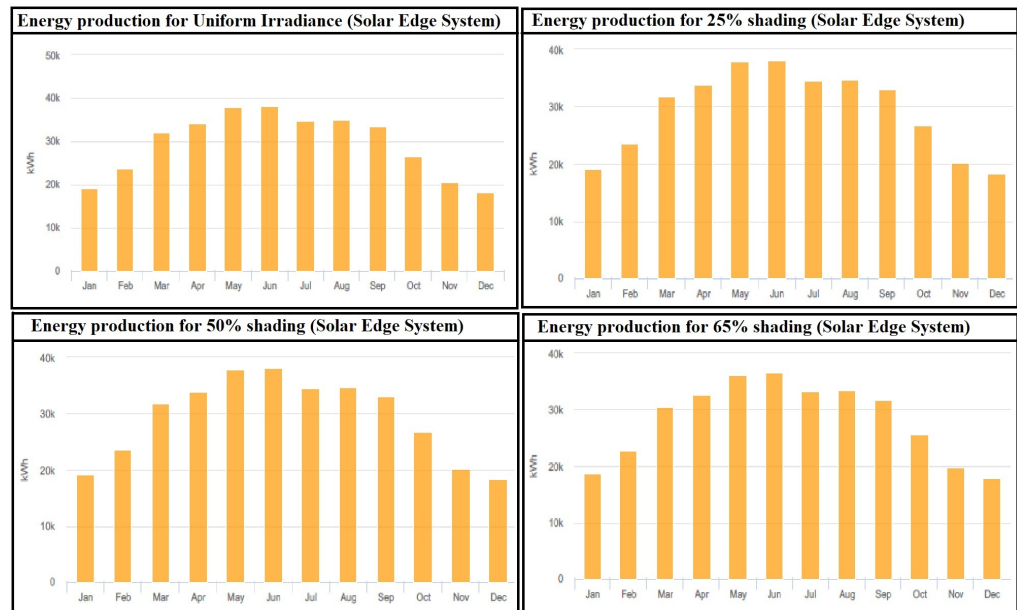


Figure 42. Results of energy production of Solar edge system on different shading conditions using Helioscope.

9.4. Huawei Centralized System

Further, after computing the result through a power optimizer, we can verify our result with a simple inverter of Huawei without an optimizer and implement this on a 239 kW system and prove through the result that a power optimizer makes the system more efficient in the case of partial shading, and the result of losses is shown in figures below. Case 1 shows the uniform irradiance having losses can be described as shading losses will be 0.0%, reflection losses are 3.9%, soiling 2.0%, irradiance losses in case of uniform is 0.5% temperature losses will be 6.5% according to the graph, Mismatch losses can be 0.2%, clipping losses 0.1%, wiring 0.4%, Inverters 1.7%, and AC system 0.5%. Case 2 expresses the 25% shading result, and the losses are as follows: shading losses will be 0.0%, reflection losses are 3.9%, soiling 2.0%, and irradiance losses. In case 2, 0.6% temperature losses will be 6.8% according to the graph, Mismatch losses can be 25.0%, wiring 0.4%, Inverters 1.7%, and AC system 0.5% can be shown in the Figure 43. Additionally, 50% shading can be considered for the result, and their losses are as follows: shading losses will be 0.0%, reflection losses are 3.9%, soiling 2.0%, irradiance losses in case 3 are 0.4%, temperature losses will be 6.8% according to the graph, Mismatch losses can be 25.0%, wiring 0.4%, Inverters 2.0%, and AC system 0.5%. In case 4, 65% shading has been considered for the result, and the losses are as follows: shading losses will be 0.0%, reflection losses are 3.9%, soiling 2.0%. Irradiance losses in case 4 are 0.7%, temperature losses are 7.8% according to the graph, Mismatch losses can be 36.6%, wiring 0.4%, Inverters 1.7% and optimizer 4.0%.

Energy production per month and year bases are described with the level of irradiance shown below in the figures. Additionally, the performance ratio on the basis of production can also be discussed with the help of irradiance different cases. Case 1 shows the uniform irradiance having a performance ratio of 85.2% with an annual production of 351.6 MWh with two field segments with maximum production in June and minimum production in January. The production graph for the uniform irradiance. While Case 2 illustrates the 25% shading having a performance ratio of 63.8% having an annual production of 263.4 MWh with two field segments with maximum production in June and minimum production in January. In Figure 44, case 3 shows the 50% shading having a performance ratio of 63.8% with an annual production of 363.2 MWh with two field segments with maximum production in June and minimum production in January. Case 4 describes the 35% irradiance having a performance ratio of 53.5% with an annual production of

220.7 MWh with two field segments with maximum production in June and minimum production in January.

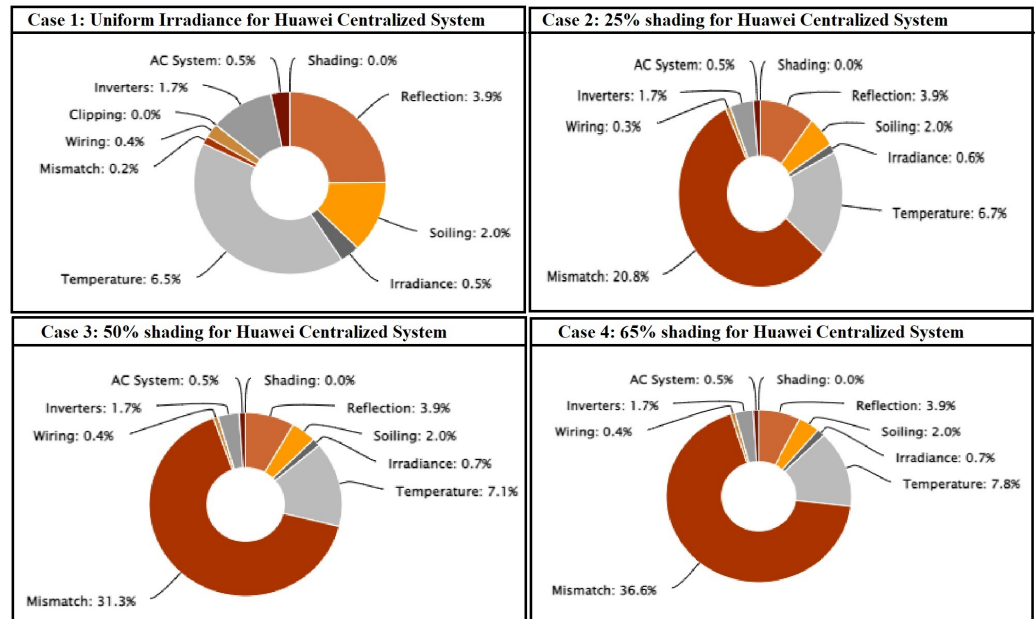


Figure 43. Results of various losses of Huawei centralized system on different shading conditions using Helioscope.

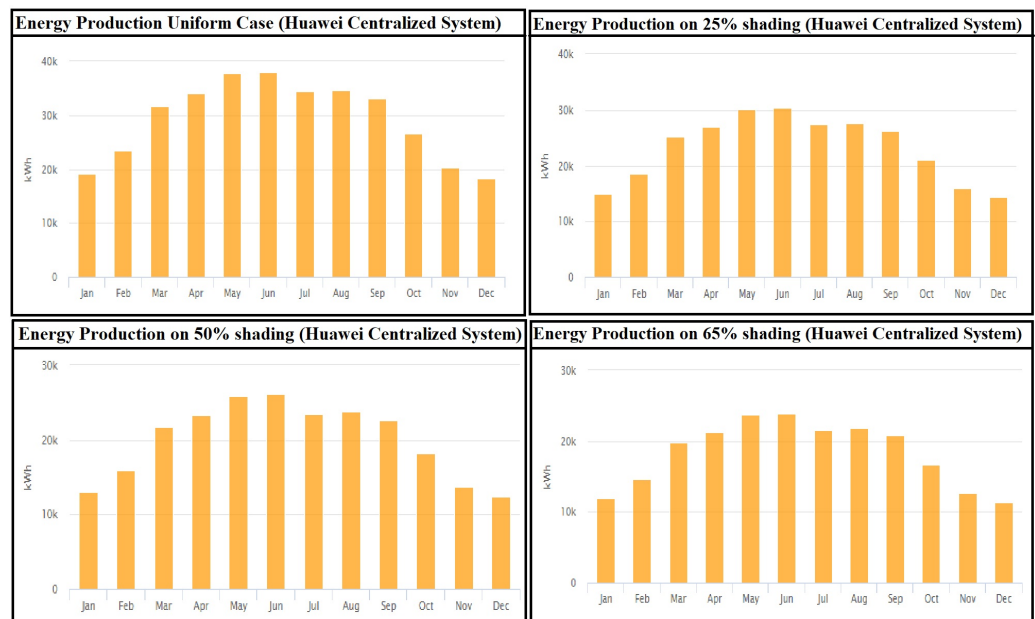


Figure 44. Results of energy production of Huawei centralized system on different shading conditions using Helioscope.

9.5. MLPE with the Help of Enphase Inverter

In order to test the Enphase optimizer, a 251 kW system has 393 modules, with itself optimizer used for synchronization. Enphase inverter makes the system more efficient in the case of partial shading the result of losses. Case 1 shows the uniform irradiance having losses can be described as shading losses will be 0.0%, reflection losses are 3.9%, soiling 2.0%, irradiance losses in case of uniform are 0.5%, temperature losses will be 6.3% according to the graph Mismatch losses can be 0.1%, wiring 0.0%, Inverters 2.6% and AC system 1.6%. In case 2, 25% shading can be considered for the result, and the

losses are as follows: shading losses will be 0.0%, reflection losses are 3.9%, soiling 2.0%, irradiance losses in case 2 are 0.6%, temperature losses will be 6.5% according to the graph, Mismatch losses can be 0.1%, wiring 0.0%, Inverters 2.6%, and AC system 1.6% have been elaborated in Figure 45. Additionally, 50% shading can be considered for the result and the losses are as follows: shading losses will be 0.0%, reflection losses are 3.9%, soiling 2.0%, irradiance losses in case 3 are 0.7%, temperature losses will be 6.9% according to the graph, Mismatch losses can be 0.1%, wiring 0.0%, Inverters 2.6%, and AC system 1.6% are shown in Figure 45. In case 4, 65% shading has been assumed for the result and the losses are as follows: shading losses will be 0.0%, reflection losses are 3.9%, soiling 2.0%, irradiance losses in case 4 are 0.7%; temperature losses will be 7.5% according to the graph, Mismatch losses can be 0.1%, wiring 0.0%, Inverters 2.6% and AC system 1.6%.

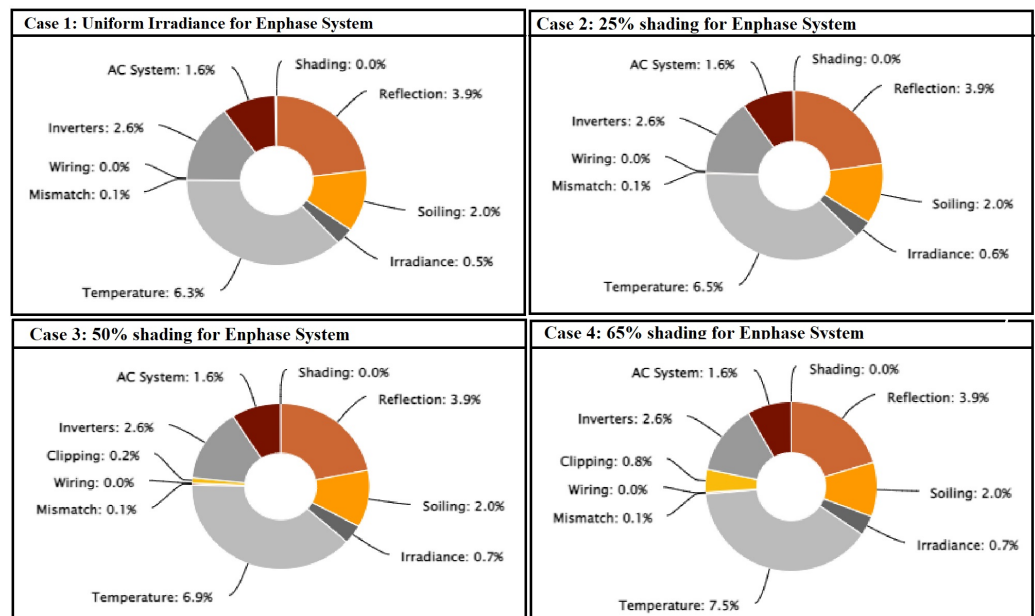


Figure 45. Results of various losses of Enphase inverter on different shading conditions using Helioscope.

Energy production per month and year bases are described with the level of irradiance shown below in the figures. Additionally, the performance ratio on the basis of production can also be discussed with the help of different irradiance cases. Case 1 shows the uniform irradiance having a performance ratio of 84.1% having an annual production of 364.0 MWh with two field segments with maximum production in June and minimum production in January. While Case 2 illustrates the 25% shading having a performance ratio of 83.7% with an annual production of 363.13 MWh with two field segments with maximum production in June and minimum production in January. Case 3 describes the 50% shading having a performance ratio of 81.8% with an annual production of 360.6 MWh with two field segments with maximum production in June and minimum production in January. At last, in Figure 46, case 4 shows the 65% shading having a performance ratio of 82.5% with an annual production of 357.1 MWh with two field segments with maximum production in June and minimum production in January.

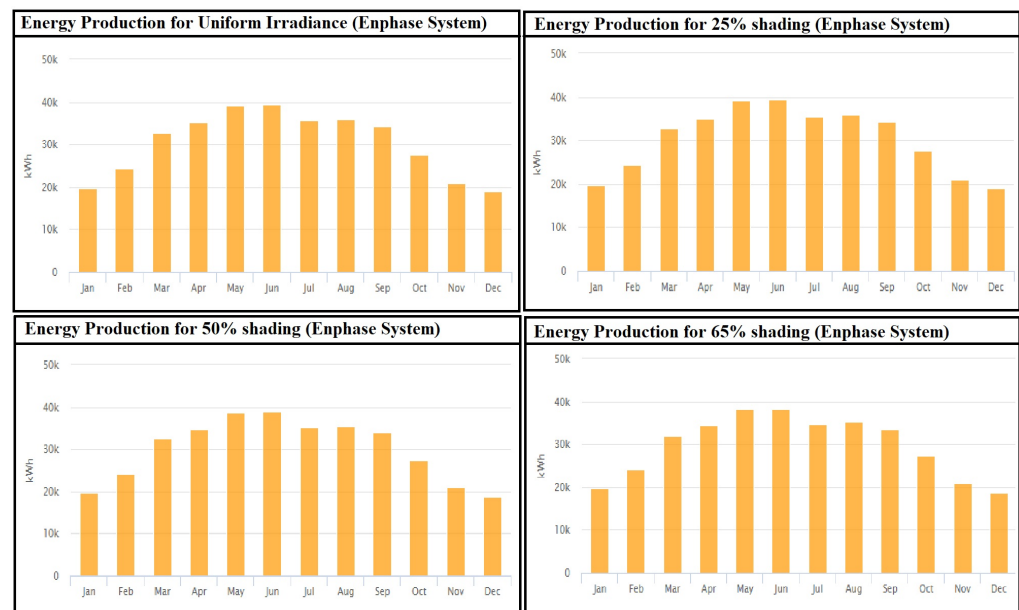


Figure 46. Results of energy production of Enphase inverter on different shading conditions using Helioscope.

9.6. Conclusion of Helioscope Result

From all six configurations, it is concluded that the power optimizer (MLPE) performs admirably in PS cases and consumes the least amount of power. To demonstrate our findings, we must create a table in which various companies' inverters and power optimizers must be displayed both with and without optimizers, and testing can be conducted under varying irradiance conditions. Table 6 shows a comparison of several firms' centralized and distributed PV systems.

Table 6. Comparison table for the Simulink model.

Company Inverter	kW System	Power Optimizer	Shading (%)	Production Monthly (kWh)
Huawei	244	Tigo	0	355,777
			65	332,747
			50	330,739
			25	302,378
Huawei	244	Huawei	0	349,762
			65	348,986
			50	347,986
			25	339,611
Solar Edge	244	Solar Edge	0	353,452
			65	352,588
			50	351,588
			25	339,873
Enphase	251	Itself	0	364,057
			65	363,138
			50	360,567
			25	357,125
Huawei	239	No	0	351,611
			65	278,477
			50	240,246
			25	220,719

For all six configurations, it is concluded that the power optimizer/MLPE works excellently in the shading cases, and minimum power can be used to show our result. A table where different companies' inverters and power optimizers have to be shown

with or without optimizer and testing can be done on various irradiance conditions. The comparison of different companies for centralized and distributed PV systems is shown in Table 6 below, where both configurations may be assessed under different irradiance conditions, and different types of PV systems can be put on the roof in accordance with their specifications, and monthly generation can be compared. Additionally, in comparison to a centralized system, we must infer that the distributed PV architecture is effective and that power could be restored.

10. Conclusions

This study evaluates two PV topologies such as centralized and distributed PV systems for uniform and partial shading conditions. In this research work, an MLPE-based converter is designed and implemented by using the DFO technique for MPP tracking. The robustness of the proposed technique is evaluated by comparing its results with Cuckoo Search (CS), Fruit Fly Optimization (FFO), Particle swarm optimization (PSO), Incremental conductance (InC) and perturb and observe (P&O) techniques. The results indicate that the proposed technique shows superior performance in terms of convergence speed and efficiency. Four different scenarios are implemented for uniform and partial shading conditions. Finally, a Helioscope-based model was simulated for MLPE and centralized system by using inverters of different companies like SMA, Tigo, Enphase, Solar edge, and Huawei. The results prove that MLPE is a better option in the case of shading region for attaining maximum power point almost 25% to 35% more power is generated through a MLPE-based system.

11. Future Work

In future work, these two topologies can be implemented on the hardware and tested in real-time scenarios as the software has its own limitations. DFO works best in the PS, and it also requires less time and computational power. In the future, we will develop or modify this technique with more reliable results for both partial shading and complex PS condition. Moreover, we will try to reduce its convergence time in all scenarios.

Author Contributions: Conceptualization, S.S., M.Y.J., M.T.N. and M.H.J.; methodology, S.S., M.Y.J., M.T.N. and M.S.A.; software, S.S., M.Y.J., M.T.N. and M.H.J.; validation, S.S., M.Y.J., M.T.N. and M.S.A.; formal analysis, S.S., M.Y.J. and M.H.J.; investigation, S.S., M.S.A., M.A.H. and M.T.N.; resources, S.S., M.Y.J. and M.S.A.; data curation, S.S., M.Y.J. and M.S.A.; writing—original draft preparation, S.S., M.Y.J. and M.T.N.; writing—review and editing, S.S., M.S.A. and M.Y.J.; visualization, S.S., M.Y.J., M.A.H. and M.T.N.; supervision, M.Y.J., M.H.J. and S.S.; project administration, M.S.A. and M.Y.J.; funding acquisition, M.S.A. All authors have read and agreed to the published version of the manuscript.

Funding: This research received no external funding.

Institutional Review Board Statement: Not applicable.

Informed Consent Statement: Not applicable.

Data Availability Statement: Not applicable.

Conflicts of Interest: The authors declare no conflict of interest.

References

1. Aldosary, A.; Ali, Z.M.; Alhaidar, M.M.; Ghahremani, M.; Dadfar, S.; Suzuki, K. A modified shuffled frog algorithm to improve MPPT controller in PV System with storage batteries under variable atmospheric conditions. *Control. Eng. Pract.* **2021**, *112*, 104831. [[CrossRef](#)]
2. Boghdady, T.A.; Kotb, Y.E.; Aljumah, A.; Sayed, M.M. Comparative Study of Optimal PV Array Configurations and MPPT under Partial Shading with Fast Dynamical Change of Hybrid Load. *Sustainability* **2022**, *14*, 2937. [[CrossRef](#)]
3. Naderipour, A.; Abdul-Malek, Z.; Nowdeh, S.A.; Kamyab, H.; Ramtin, A.R.; Shahrokhi, S.; Klemeš, J.J. Comparative evaluation of hybrid photovoltaic, wind, tidal and fuel cell clean system design for different regions with remote application considering cost. *J. Clean. Prod.* **2021**, *283*, 124207. [[CrossRef](#)]

4. Hussain, M.; Butt, A.R.; Uzma, F.; Ahmed, R.; Irshad, S.; Rehman, A.; Yousaf, B. A comprehensive review of climate change impacts, adaptation, and mitigation on environmental and natural calamities in Pakistan. *Environ. Monit. Assess.* **2020**, *192*, 1–20. [[CrossRef](#)]
5. Abbass, K.; Qasim, M.Z.; Song, H.; Murshed, M.; Mahmood, H.; Younis, I. A review of the global climate change impacts, adaptation, and sustainable mitigation measures. *Environ. Sci. Pollut. Res.* **2022**, *29*, 42539–42559. [[CrossRef](#)]
6. Wasim, M.S.; Amjad, M.; Habib, S.; Abbasi, M.A.; Bhatti, A.R.; Muyeen, S. A critical review and performance comparisons of swarm-based optimization algorithms in maximum power point tracking of photovoltaic systems under partial shading conditions. *Energy Rep.* **2022**, *8*, 4871–4898. [[CrossRef](#)]
7. Sattianadan, D.; Gorai, S.; Kumar, G.P.; Vidyasagar, S.; Shanmugasundaram, V. Potency of PR controller for multiple harmonic compensation for a single-phase grid connected system. *Int. J. Power Electron. Drive Syst.* **2020**, *11*, 1491. [[CrossRef](#)]
8. Huang, Y.P.; Hsu, S.Y. A performance evaluation model of a high concentration photovoltaic module with a fractional open circuit voltage-based maximum power point tracking algorithm. *Comput. Electr. Eng.* **2016**, *51*, 331–342. [[CrossRef](#)]
9. Nadeem, A.; Sher, H.A.; Murtaza, A.F.; Ahmed, N. Online current-sensorless estimator for PV open circuit voltage and short circuit current. *Solar Energy* **2021**, *213*, 198–210. [[CrossRef](#)]
10. Karabacak, M. A new perturb and observe based higher order sliding mode MPPT control of wind turbines eliminating the rotor inertial effect. *Renew. Energy* **2019**, *133*, 807–827. [[CrossRef](#)]
11. Nkambule, M.S.; Hasan, A.N.; Ali, A. MPPT under partial shading conditions based on Perturb & Observe and Incremental Conductance. In Proceedings of the 2019 11th International Conference on Electrical and Electronics Engineering (ELECO), Bursa, Turkey, 28–30 November 2019; pp. 85–90.
12. Hota, A.; Bhuyan, S.K.; Hota, P.K. Modeling & simulation of photovoltaic system connected to grid using Matlab. In Proceedings of the 2020 International Conference on Renewable Energy Integration into Smart Grids: A Multidisciplinary Approach to Technology Modelling and Simulation (ICREISG), Bhubaneswar, India, 14–15 February 2020; pp. 16–21.
13. Dhass, A.; Beemkumar, N.; Hari Krishnan, S.; Ali, H.M. A Review on Factors Influencing the Mismatch Losses in Solar Photovoltaic System. *Int. J. Photoenergy* **2022**, *2022*, 2986004. [[CrossRef](#)]
14. Parthasarathy, K.; Vijayaraj, S.; Radhakrishnan, G.; Leemarose, J.; Rajesh, K. Implementation of solar power optimizer to enhance output power of a solar PV plant. *Nat. Volatiles Essent.* **2021**, *8*, 1561–1567.
15. Fan, L.; Ma, X. Maximum power point tracking of PEMFC based on hybrid artificial bee colony algorithm with fuzzy control. *Sci. Rep.* **2022**, *12*, 4316. [[CrossRef](#)]
16. Phanden, R.K.; Sharma, L.; Chhabra, J.; Demir, H.İ. A novel modified ant colony optimization based maximum power point tracking controller for photovoltaic systems. *Mater. Today Proc.* **2021**, *38*, 89–93. [[CrossRef](#)]
17. Restrepo-Cuestas, B.J.; Montano, J.; Ramos-Paja, C.A.; Trejos-Grisales, L.A.; Orozco-Gutierrez, M.L. Parameter Estimation of the Bishop Photovoltaic Model Using a Genetic Algorithm. *Appl. Sci.* **2022**, *12*, 2927. [[CrossRef](#)]
18. Tajuddin, M.; Azmi, A.; Ayob, S.; Sutikno, T. Differential evolution based solar photovoltaic array reconfiguration algorithm for optimal energy extraction during partial shading condition. *Int. J. Power Electron. Drive Syst.* **2018**, *9*, 1397.
19. Suhardi, D.; Syafaah, L.; Irfan, M.; Yusuf, M.; Effendy, M.; Pakaya, I. Improvement of maximum power point tracking (MPPT) efficiency using grey wolf optimization (GWO) algorithm in photovoltaic (PV) system. In Proceedings of the IOP Conference Series: Materials Science and Engineering, Kazimierz Dolny, Poland, 23–25 July 2019; IOP Publishing: Bristol, UK, 2019; Volume 674, p. 012038.
20. Hussaian Basha, C.; Bansal, V.; Rani, C.; Brisilla, R.; Odofin, S. Development of cuckoo search MPPT algorithm for partially shaded solar PV SEPIC converter. In *Soft Computing for Problem Solving*; Springer: Berlin/Heidelberg, Germany, 2020; pp. 727–736.
21. Kamil, A.A.; Nasr, M.S.; Alwash, S. Maximum Power Point Tracking Method for Photovoltaic System Based on Enhanced Particle Swarm Optimization Algorithm Under Partial Shading Condition. *Int. J. Intell. Eng. Syst.* **2020**, *13*, 241–254. [[CrossRef](#)]
22. Pei, T.; Hao, X.; Gu, Q. A novel global maximum power point tracking strategy based on modified flower pollination algorithm for photovoltaic systems under non-uniform irradiation and temperature conditions. *Energies* **2018**, *11*, 2708. [[CrossRef](#)]
23. Kayri, I.; Gencoglu, M.T. Predicting power production from a photovoltaic panel through artificial neural networks using atmospheric indicators. *Neural Comput. Appl.* **2019**, *31*, 3573–3586. [[CrossRef](#)]
24. Shahdadi, A.; Khajeh, A.; Barakati, S.M. A new slip surface sliding mode controller to implement MPPT method in photovoltaic system. In Proceedings of the 2018 9th Annual Power Electronics, Drives Systems and Technologies Conference (PEDSTC), Tehran, Iran, 13–15 February 2018; pp. 212–217.
25. Jin, Y.; Hou, W.; Li, G.; Chen, X. A glowworm swarm optimization-based maximum power point tracking for photovoltaic/thermal systems under non-uniform solar irradiation and temperature distribution. *Energies* **2017**, *10*, 541. [[CrossRef](#)]
26. Afzal Awan, M.M.; Mahmood, T. A novel ten check maximum power point tracking algorithm for a standalone solar photovoltaic system. *Electronics* **2018**, *7*, 327. [[CrossRef](#)]
27. Hosseinpour, M.; Mansoori, S.; Shayeghi, H. Selective Harmonics Elimination Technique in Cascaded H-Bridge Multi-Level Inverters Using the Salp Swarm Optimization Algorithm. *J. Oper. Autom. Power Eng.* **2020**, *8*, 32–42.
28. Awan, M.M.A.; Javed, M.Y.; Asghar, A.B.; Ejsmont, K. Performance Optimization of a Ten Check MPPT Algorithm for an Off-Grid Solar Photovoltaic System. *Energies* **2022**, *15*, 2104. [[CrossRef](#)]
29. Kumar, N.; Hussain, I.; Singh, B.; Panigrahi, B.K. Rapid MPPT for uniformly and partial shaded PV system by using JayaDE algorithm in highly fluctuating atmospheric conditions. *IEEE Trans. Ind. Inform.* **2017**, *13*, 2406–2416. [[CrossRef](#)]

30. Lin, Z.; Wang, J.; Fang, Z.; Hu, M.; Cai, C.; Zhang, J. Accurate maximum power tracking of wireless power transfer system based on simulated annealing algorithm. *IEEE Access* **2018**, *6*, 60881–60890. [[CrossRef](#)]
31. Yang, X.; Li, W.; Su, L.; Wang, Y.; Yang, A. An improved evolution fruit fly optimization algorithm and its application. *Neural Comput. Appl.* **2020**, *32*, 9897–9914. [[CrossRef](#)]
32. Omar, A.; Hasanien, H.M.; Elgendy, M.A.; Badr, M.A. Identification of the photovoltaic model parameters using the crow search algorithm. *J. Eng.* **2017**, *2017*, 1570–1575. [[CrossRef](#)]
33. Heidari, A.A.; Mirjalili, S.; Faris, H.; Aljarah, I.; Mafarja, M.; Chen, H. Harris hawks optimization: Algorithm and applications. *Future Gener. Comput. Syst.* **2019**, *97*, 849–872. [[CrossRef](#)]
34. Poonahela, I.; Bayhan, S.; Abu-Rub, H.; Begovic, M.M.; Shadmand, M.B. An effective finite control set-model predictive control method for grid integrated solar PV. *IEEE Access* **2021**, *9*, 144481–144492. [[CrossRef](#)]
35. Radhika, S.; Margaret, V. A Review on DC-DC Converters with Photovoltaic System in DC Micro Grid. *J. Phys. Conf. Ser.* **2021**, *1804*, 012155. [[CrossRef](#)]
36. Gharechahi, A.; Shahrezayi, A.J.; Hamzeh, M.; Afjei, E. Increasing of Harvested Power in DMPPT-based PV Systems by a New Scan Method. In Proceedings of the 2022 13th Power Electronics, Drive Systems, and Technologies Conference (PEDSTC), Tehran, Iran, 1–3 February 2022; pp. 592–597.
37. Ku, C.Y.; Noranai, Z. Case study of solar PV comparison cost saving at student accommodation. *Res. Prog. Mech. Manuf. Eng.* **2021**, *2*, 57–63.
38. Kabalci, E. Review on novel single-phase grid-connected solar inverters: Circuits and control methods. *Sol. Energy* **2020**, *198*, 247–274. [[CrossRef](#)]
39. Ali, A.I.; Sayed, M.A.; Mohamed, E.E. Modified efficient perturb and observe maximum power point tracking technique for grid-tied PV system. *Int. J. Electr. Power Energy Syst.* **2018**, *99*, 192–202. [[CrossRef](#)]
40. Donadi, A.K.; Jahnavi, W. Review of DC-DC Converters in Photovoltaic Systems for MPPT Systems. *Int. Res. J. Eng. Technol. (IRJET)* **2019**, *6*, 1914–1918.
41. Trejo, D.R.E.; Taheri, S.; Saavedra, J.L.; Vázquez, P.; De Angelo, C.H.; Pecina-Sánchez, J.A. Nonlinear Control and Internal Stability Analysis of Series-Connected Boost DC/DC Converters in PV Systems With Distributed MPPT. *IEEE J. Photovolt.* **2020**, *11*, 504–512. [[CrossRef](#)]
42. Raghavendra, K.V.G.; Zeb, K.; Muthusamy, A.; Krishna, T.; Kumar, S.; Kim, D.H.; Kim, M.S.; Cho, H.G.; Kim, H.J. A comprehensive review of DC-DC converter topologies and modulation strategies with recent advances in solar photovoltaic systems. *Electronics* **2020**, *9*, 31. [[CrossRef](#)]
43. Choudhury, T.R.; Nayak, B.; De, A.; Santra, S.B. A comprehensive review and feasibility study of DC-DC converters for different PV applications: ESS, future residential purpose, EV charging. *Energy Syst.* **2020**, *11*, 641–671. [[CrossRef](#)]
44. Amir, A.; Amir, A.; Che, H.S.; Elkhateb, A.; Abd Rahim, N. Comparative analysis of high voltage gain DC-DC converter topologies for photovoltaic systems. *Renew. Energy* **2019**, *136*, 1147–1163. [[CrossRef](#)]
45. Krishnamurthy, K.; Padmanaban, S.; Blaabjerg, F.; Neelakandan, R.B.; Prabhu, K.R. Power electronic converter configurations integration with hybrid energy sources—a comprehensive review for state-of-the-art in research. *Electr. Power Compon. Syst.* **2019**, *47*, 1623–1650. [[CrossRef](#)]
46. Farh, H.M.; Eltamaly, A.M. Maximum power extraction from the photovoltaic system under partial shading conditions. In *Modern Maximum Power Point Tracking Techniques for Photovoltaic Energy Systems*; Springer: Berlin/Heidelberg, Germany, 2020; pp. 107–129.
47. Ponnusamy, P.; Sivaraman, P.; Almakhlis, D.J.; Padmanaban, S.; Leonowicz, Z.; Alagu, M.; Ali, J.S.M. A new multilevel inverter topology with reduced power components for domestic solar PV applications. *IEEE Access* **2020**, *8*, 187483–187497. [[CrossRef](#)]
48. Pant, S.; Saini, R. Comparative study of MPPT techniques for solar photovoltaic system. In Proceedings of the 2019 International Conference on Electrical, Electronics and Computer Engineering (UPCON), Piscataway, NJ, USA, 8–10 November 2019; pp. 1–6.
49. Khosrojerdi, F.; Golkhandan, N.H. Microcontroller-based maximum power point tracking methods in photovoltaic systems. In Proceedings of the 2018 9th Annual Power Electronics, Drives Systems and Technologies Conference (PEDSTC), Tehran, Iran, 13–15 February 2018; pp. 330–334.
50. Javed, M.R.; Waleed, A.; Riaz, M.T.; Virk, U.S.; Ahmad, S.; Daniel, K.; Hussan, U.; Khan, M.A. A Comparative Study of Maximum Power Point Tracking Techniques for Solar Systems. In Proceedings of the 2019 22nd International Multitopic Conference (INMIC), Islamabad, Pakistan, 29–30 November 2019; pp. 1–6.
51. Ravyts, S.; Dalla Vecchia, M.; Zwysen, J.; Van den Broeck, G.; Driesen, J. Study on a cascaded DC-DC converter for use in building-integrated photovoltaics. In Proceedings of the 2018 IEEE Texas Power and Energy Conference (TPEC), College Station, TX, USA, 8–9 February 2018; pp. 1–6.
52. Lee, H.S.; Yun, J.J. Advanced MPPT algorithm for distributed photovoltaic systems. *Energies* **2019**, *12*, 3576. [[CrossRef](#)]
53. Liu, L.; Meng, X.; Liu, C. A review of maximum power point tracking methods of PV power system at uniform and partial shading. *Renew. Sustain. Energy Rev.* **2016**, *53*, 1500–1507. [[CrossRef](#)]
54. Mao, M.; Cui, L.; Zhang, Q.; Guo, K.; Zhou, L.; Huang, H. Classification and summarization of solar photovoltaic MPPT techniques: A review based on traditional and intelligent control strategies. *Energy Rep.* **2020**, *6*, 1312–1327. [[CrossRef](#)]
55. Sarwar, S.; Javed, M.Y.; Jaffery, M.H.; Arshad, J.; Ur Rehman, A.; Shafiq, M.; Choi, J.G. A Novel Hybrid MPPT Technique to Maximize Power Harvesting from PV System under Partial and Complex Partial Shading. *Appl. Sci.* **2022**, *12*, 587. [[CrossRef](#)]

56. Sarwar, S.; Hafeez, M.A.; Javed, M.Y.; Asghar, A.B.; Ejsmont, K. A Horse Herd Optimization Algorithm (HOA)-Based MPPT Technique under Partial and Complex Partial Shading Conditions. *Energies* **2022**, *15*, 1880. [[CrossRef](#)]
57. Javed, M.Y.; Hasan, A.; Rizvi, S.T.H.; Hafeez, A.; Sarwar, S.; Telmoudi, A.J. Water Cycle Algorithm (WCA): A New Technique to Harvest Maximum Power from PV. *Cybern. Syst.* **2022**, *53*, 80–102. [[CrossRef](#)]
58. Deline, C.; Meydbray, J.; Donovan, M. *Photovoltaic Shading Testbed for Module-Level Power Electronics: 2016 Performance Data Update*; Technical Report; National Renewable Energy Lab. (NREL): Golden, CO, USA, 2016.
59. Geyer, T.; Quevedo, D.E. Multistep finite control set model predictive control for power electronics. *IEEE Trans. Power Electron.* **2014**, *29*, 6836–6846. [[CrossRef](#)]
60. Ahmad, R.; Murtaza, A.F.; Sher, H.A.; Shami, U.T.; Olalekan, S. An analytical approach to study partial shading effects on PV array supported by literature. *Renew. Sustain. Energy Rev.* **2017**, *74*, 721–732. [[CrossRef](#)]
61. Mirjalili, S. Dragonfly algorithm: A new meta-heuristic optimization technique for solving single-objective, discrete, and multi-objective problems. *Neural Comput. Appl.* **2016**, *27*, 1053–1073. [[CrossRef](#)]
62. Saravanan, S.; Babu, N.R. Maximum power point tracking algorithms for photovoltaic system—A review. *Renew. Sustain. Energy Rev.* **2016**, *57*, 192–204. [[CrossRef](#)]
63. Ghasemi, M.A.; Foroushani, H.M.; Blaabjerg, F. Marginal power-based maximum power point tracking control of photovoltaic system under partially shaded condition. *IEEE Trans. Power Electron.* **2019**, *35*, 5860–5872. [[CrossRef](#)]
64. Bharath, K. A novel modified ant colony optimization based maximum power point tracking controller for photovoltaic systems A novel sensorless hybrid MPPT method based on FOCV measurement and P&O MPPT technique for solar PV applications. In Proceedings of the 2019 International Conference on Advances in Computing and Communication Engineering (ICACCE), Sathyamangalam, India, 4–6 April 2019; pp. 1–5.
65. Huynh, D.C.; Dunnigan, M.W. Development and comparison of an improved incremental conductance algorithm for tracking the MPP of a solar PV panel. *IEEE Trans. Sustain. Energy* **2016**, *7*, 1421–1429. [[CrossRef](#)]